Journal of Medicinal Chemistry

Article

Integrated Strategies for Identifying Leads that Target the NS3 Helicase of the Hepatitis C Virus

Steven R. LaPlante, Anil Padyana, Asitha Abeywardnae, Pierre R Bonneau, Mireille Cartier, Rene Colombe, Araz Jakalian, Jessi Jones, Xiang Li, Shuang Liang, Ginette McKercher, Peter W White, Qiang Zhang, and Steven J. Taylor

J. Med. Chem., **Just Accepted Manuscript** • Publication Date (Web): 07 Jan 2014

Just Accepted

Journal of Medicinal Chemistry is published by the American Chemical Society. 1155 Sixteenth Street N.W., Washington, DC 20036

Integrated Strategies for Identifying Leads that Target the NS3 Helicase of the Hepatitis C Virus

Steven R. LaPlante*,[1] Anil K. Padyana,[2] Asitha Abeywardane,[2] Pierre Bonneau,[1] Mireille Cartier,[1] René Coulombe,[1] Araz Jakalian,[1] Jessi Wildeson-Jones,[3] Xiang Li,[2] Shuang Liang,[2]Ginette McKercher,[1] Peter White,[1] Qiang Zhang,[2] Steven J. Taylor[2]

.

[1]Departments of Chemistry and Biological Sciences, Boehringer Ingelheim (Canada) Ltd, R&D, 2100 Cunard Street, Laval, Québec, H7S 2G5, CANADA.

[2]Department of Medicinal Chemistry, [3]Department of Biotherapeutics, 900 Ridgebury Road, Boehringer Ingelheim Pharmaceuticals, Inc., Ridgefield, CT 06877 USA.

ABSTRACT: Future treatments for individuals infected by the hepatitis C virus (HCV) will likely involve combinations of compounds that inhibit multiple viral targets. The helicase of HCV is an attractive target with no known drug candidates in clinical trials. Herein we describe an integrated strategy for identifying fragment inhibitors using structural and biophysical techniques. Based on an X-ray structure of apo HCV helicase, *in silico* and bioinformatic analyses of HCV variants, we identified that one site in particular (labeled 3+4) was the most conserved and attractive pocket to target for a drug discovery campaign. Compounds from multiple sources were screened to identify inhibitors/binders to this site, and enzymatic and biophysical assays (NMR and/or SPR) were used to triage the most promising ligands for exploration by X-ray crystallography. Medicinal chemistry and biophysical evaluations focused on exploring the most promising lead series. The strategies employed here can have general utility in drug discovery.

INTRODUCTION

Chronic hepatitis C virus (HCV) infection is a serious health problem affecting approximately 2-3% of the world population.[1] Left untreated, HCV infection can lead to extensive liver damage such as cirrhosis and hepatocarcinomas, ultimately leading to liver failure and/or cancer.[1b] Intense research into treatments for HCV has been ongoing since the discovery of the virus in 1989.[2] Until recently, the only therapies available were combinations of non-specific immune modulatory agents (pegylated interferon and ribavirin), which have limited efficacy and severe side-effects particularly against major genotype 1.[3] The first two HCV-specific antivirals, inhibitors of the viral serine protease NS3, were approved in 2011, and 2nd generation protease inhibitors are in late stage development or recently approved.[4] However, to minimize the emergence of resistance, the protease inhibitors are still co-administered with interferon (IFN) and ribavirin.[5] Results from recent trials suggest that combinations of multiple antivirals targeting complementary HCV targets, with or without ribavirin, will be needed to remove interferon from standard treatment regimens, particularly for genotype 1 (GT-1)[6]. Recently, sofosbuvir, which is an NS5B polymerase inhibitor, was recently approved for IFN-free GT-2 and GT-3.

HCV has a small genome encoding five nonstructural proteins, including four distinct enzymatic activities that have been the focus of extensive research for development of therapies.[7] In addition to the NS3 protease, several classes of inhibitors for the viral RNA-dependent RNA polymerase are in late-stage clinical trials.[8] The other two enzymatic activities are autoproteolysis of the NS2-NS3 junction by a cysteine protease domain of NS2, and ATP-dependent RNA unwinding activity encoded by the C-terminal two-thirds of the bi-functional NS3 helicase protein. There are few reports of inhibitors for either of these activities, and to our

knowledge none have advanced to clinical development. NS2-NS3 activity is inherently difficult to assay,[9,10] and it is not surprising that little progress has been reported with this potential target. In comparison, helicase activity is relatively straight-forward to evaluate, and this target has been widely screened. However, very few viral-specific inhibitors have been reported, and most have been found to act via undesirable mechanisms (e.g. nonspecific binding to the nucleic acid substrate instead of the protein, or interfering with the assay signal).[11,12, 13f] Despite this limited success, there is an abundance of structural and mechanistic information on this helicase,[13,14] and no obvious reason why helicase would not be druggable.

In this work, we describe our structure based drug discovery efforts to target this essential HCV enzyme. We started by evaluating the druggability of this protein, and determined that efforts were to focus exclusively at the most conserved site (labeled as site 3+4) near amino acid residue W501. Compound screening and subsequent triaging of the hits employed strategic biophysical methods and specificity counterscreens, which led to nine series of compounds. Prioritization processes then afforded the indole series which provided potent and attractive leads based on encouraging structure activity relationship (SAR) trends, stoichiometry of binding, mechanism of inhibition and favorable solution property behavior.

RESULTS AND DISCUSSION

HCV Helicase Druggability and Analysis of Potential Ligand Binding Pockets. HCV helicase is known to unwind double-stranded RNA in a NTP-dependent fashion, and this activity can be stimulated *in vitro* by the addition of single stranded nucleic acid. Most RNA helicases are grouped into two major superfamilies based on the occurrence of seven to eight conserved

structural motifs which are essential to enzymatic function. Residues in those motifs contribute to either NTP or RNA binding or couple the energy of NTP hydrolysis to dsRNA unwinding activity. These conserved motifs are localized within the two N-terminal domains (see Domains I and II on the X-ray structure of HCV NS3 helicase complexed with a single-stranded DNA octamer in Figure 1).[32]

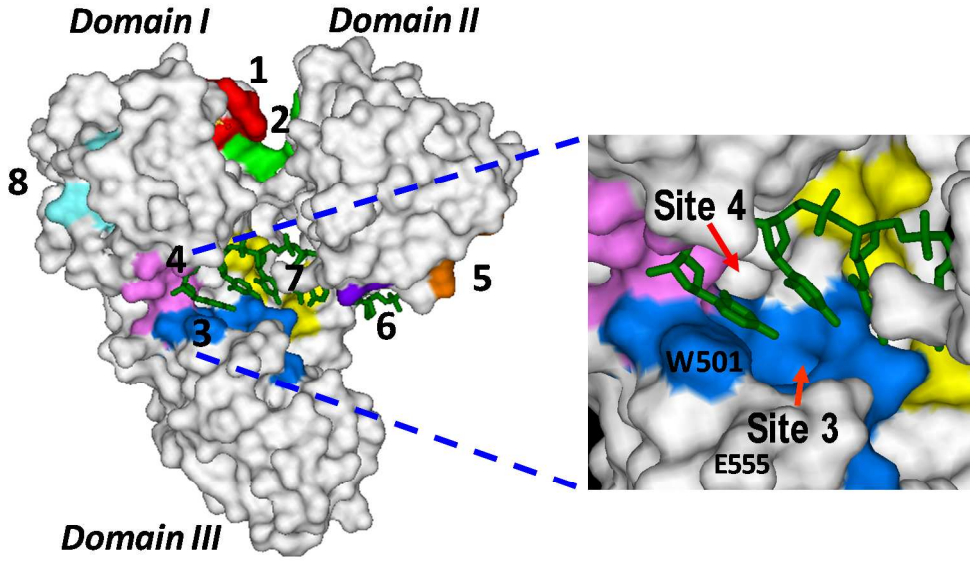

Figure 1. Solid surface view of an X-ray structure of HCV helicase bound to a DNA octamer. Shown on the left is the full view of the X-ray structure of HCV helicase with *in silico* derived annotated PASS sites (colored) which predict potential pockets and binding sites. The NTP binding site corresponds to sites 1 and 2. The zoomed view on the right displays site 3+4 with the single-stranded DNA octamer (green atoms) superposed onto the structure for visual purposes, PDB code 1A1V.[32]

Based on this X-ray structure of the HCV helicase with the DNA substrate removed, we performed an *in silico* pocket finding study using the program PASS (Putative Active Site with Spheres) in order to identify potential binding sites.[33] Our *in silico* PASS analyses identified

eight potential ligand binding sites on the three domains. Figure 1 shows these eight sites which were mostly located in regions of the conserved helicase motifs and the substrate binding regions.

Having identified sites that could theoretically accommodate small molecule inhibitors, we proceeded to assess the druggability of these sites, and the homology of these pockets across genotypes. To evaluate the potential for these issues, two additional dimensions of data were acquired for each of the residues that lined these sites. An amino acid conservation analysis was performed by comparing the sequences of 361 HCV genome sequences, and residue flexibility analysis was performed based on the crystallographic B-factors. Data for both dimensions are provided in Figure 2 for the helicase residues located within PASS sites 3 and 4 (vide infra).

PASS Site 3
(RNA binding site on domain III)

Residue	All Genotypes	Genotype 1 only	Flexibility
E493	360/361	215/216	+
D496	360/361	215/216	-
A497	346/361	214/216	-
W501	361/361	216/216	-
E555	149/361	51/216	++
N556	356/361	214/216	+
F557	296/361	196/216	-
P558	308/361	216/216	-

PASS Site 4
(RNA binding on domain I)

Residue	All Genotypes	Genotype 1 only	Flexibility
G255	361/361	216/216	-
T269	359/361	215/216	+
G271	357/361	215/216	-
K272	360/361	216/216	+
A275	361/361	216/216	-
Y502	359/361	215/216	-

Figure 2. Residue conservation and flexibility analyses of amino acids that line the PASS ligand binding sites 3 and 4. The numbers shown indicate the same residues found versus the number of viral sequences analyzed. Flexibility was based on X-ray crystallographic B-factors. Residues with higher B-factors were denoted by a "+ or ++" and suggested higher flexibility, whereas lower B-factors were denoted by a "-" and suggested lower flexibility.

Analysis of the data shows that residues in site 4 are highly conserved across genotype sequences; the same residue is noted for >350 genotypes; out of 361 studied (see the column labelled All Genotypes in Figure 2). This attractive feature suggested that this site had the potential for targeting pan-genotype activity. More variability was noted for site 3, where the bioinformatics analysis showed that residue E555 was conserved in only 149 of 361 genotypes conferred, and exhibited spatial flexibility (see ++ under the Flexibility column, Figure 2) based on its crystallographic B-factor. However, other residues in site 3 were highly conserved such as W501 which was observed in 361/361 of the genome sequences. Similar analyses on other PASS sites showed significantly more sequence heterogeneity and flexibility (see Supporting Information). Based on the above analysis, we rationalized that the most favorable opportunities for identifying a useful small molecule drug was to target exclusively sites 3 and/or 4 (3+4).

Our campaign then turned to traditional high throughput screening (HTS) as well as novel fragment based methods as lead finding approaches to target this site. As a first line of approach, we screened our corporate compound collection (>10^6 compounds) using RNA-unwinding assays with the NS3 helicase domain and the full-length NS3/NS4A heterodimer monitoring helicase activity. These campaigns identified compounds which inhibited the assay signal, but all were shown to inhibit either by substrate intercalation, interference with the readout of the assay or have some other undesirable mechanism. Ultimately, no compounds were identified that had sufficient activity, selectivity, and which also inhibitored by the desired mechanism. Without any suitable compounds identified from HTS, we transitioned to a fragment-based drug discovery (FBDD) campaign.

Fragment Screens – Various Lead Sources and Screening Methods. We then implemented an integrated FBDD strategy which involved screening compounds from various

sources to maximize opportunities to identify hit candidates to funnel through triaging filters then subsequent optimization (Figure 3). To maximize the chances of finding leads in FBDD campaign, we screened fragments from multiple sources. One source of fragments came from revisiting fragment-like hits from the earlier HTS campaigns that were rejected due to poor potency. Other sources included fragments from in-house screening collections tested in a RNA-unwinding functional assay (FA) at high compound concentrations (up to 500 μM) to allow the detection of weakly active binders. Libraries of fragments from commercial sources were also screened in a surface plasma resonance assay (SPR). In parallel, additional compounds were identified from virtual screening of in-house and external vendor compound collections, followed by functional assays (FA), then verifications by biophysical filtering methods (NMR or SPR).

Our workflow employed stringent triaging and prioritization strategies (using SPR and a toolbox of NMR methods) to identify quality binders and specific inhibitors of HCV helicase. An early objective was to prioritize quality ligands that could be funneled to X-ray crystallography studies to acquire atomic-level views of complexes with NS3 helicase. This and NMR evidence served to validate ligands that bound to site 3+4 which then triggered and enabled structure-based drug design, idea generation and analogue verification.

It was noteworthy that, in practice, this strategy was heavily burdened by false-positive hits especially given the high concentrations of compounds required for FA testing and for biophysical binding studies. At these higher concentrations, unusual physical properties and binding phenomenon were encountered (solubility, aggregation, promiscuity, *vide infra*) that adversely affected some biophysical analyses and interpretations. Therefore, specific follow-up triaging methods were implemented to eliminate compounds with such adverse properties.[29]

Overall, the functional assays, counter screens and the NMR assays proved most useful for evaluating and promoting quality hits for maximizing success in crystallization trials.

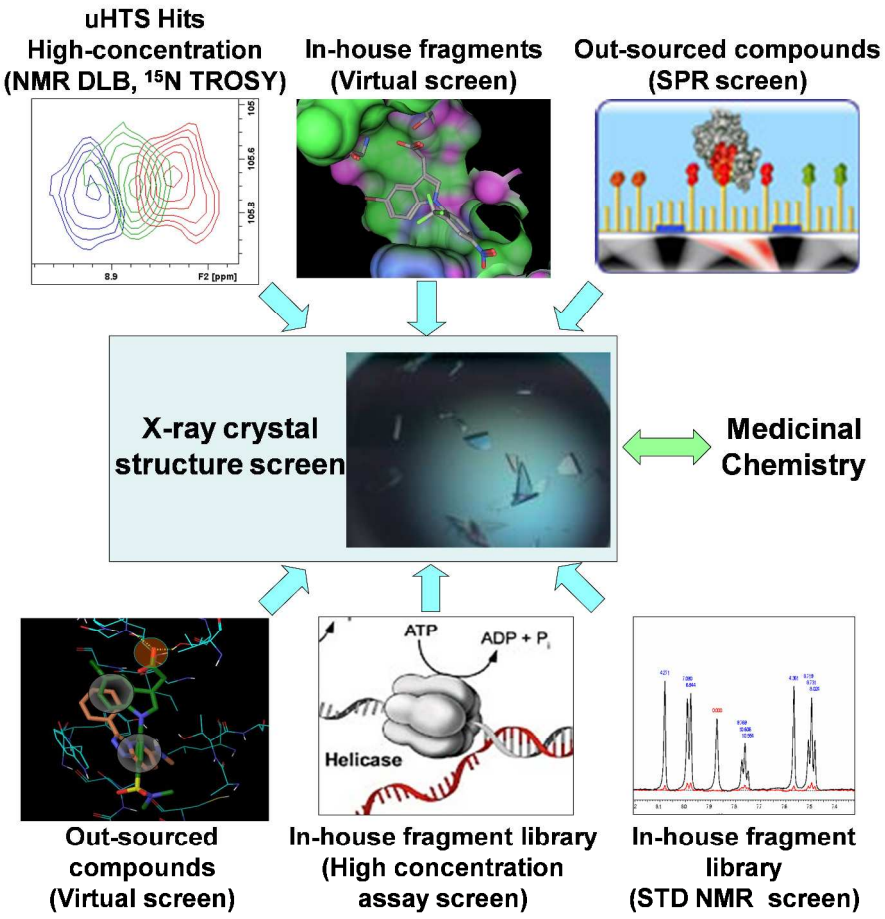

Figure 3. Screening methods and compound sources used to identify weak binding fragments for X-ray crystallography screens then medicinal chemistry.

Hit and Chemotype Classification: Binders/inhibitors identified from the workflow described above were then classified according to scaffold commonalities, and related analogues were sought (in-house and commercial) then tested. The more promising series were clustered into nine chemotypes based on the similarities of the core scaffolds as shown in Figure 4. Compounds from these series were then subjected to soaking or co-crystallization for

confirmation of binding to the desired 3+4 site. No evidence of binding to helicase was noted for series S6, S7 and S9 in crystallization trials, and therefore these were deprioritized. Compounds in series S5 were confirmed as binders to helicase, but ligand electron densities were found at sites other than site 3+4. Five chemotypes (S1-S4 and S8) were identified that were confirmed to bind to site 3+4, and thirteen examples are shown overlaid in Figure 5. The most notable feature of this superposition is that the compounds are centralized within a wide groove above W501. Some compounds hydrogen-bond to the backbone of G255 and others appear to partially enter a lipophilic pocket or interact with polar residues located in the bottom right of the pocket. Overall, the wide groove and small lipophilic pocket suggests that targeting this site and optimizing for potency could be challenging. From this point of view, chemotypes S2-S4 were considered the most promising. However, series S3 and S4 were subsequently deprioritized (see Supporting Information) and efforts were focused on the S2 indole series as described in detail below.

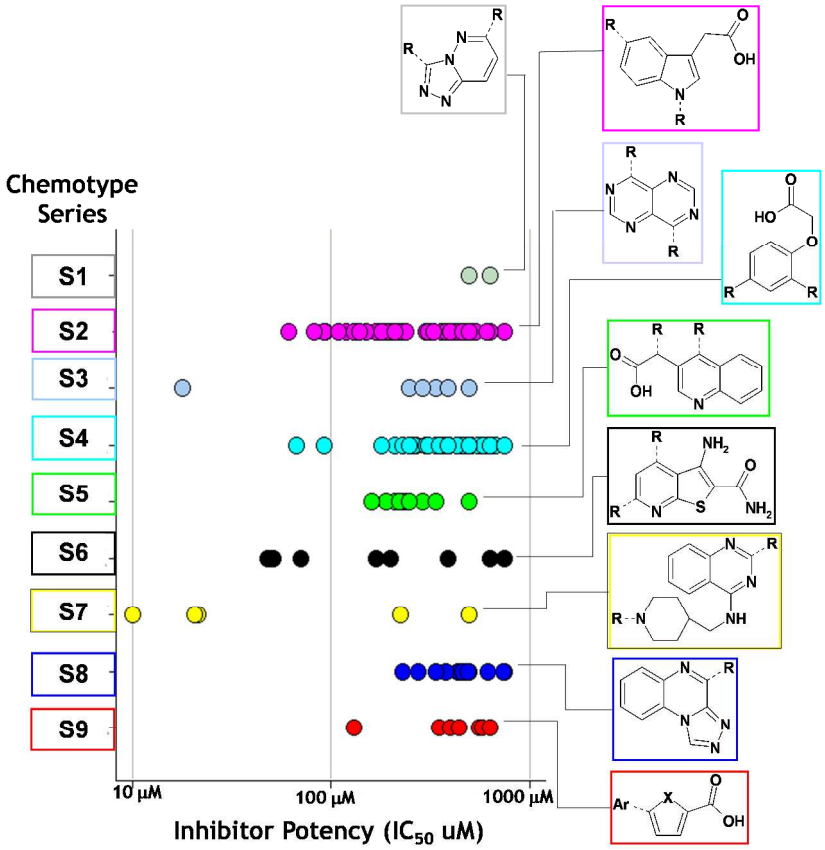

Figure 4. Shown are the chemotype series (S1-S9) and inhibitory potencies of fragment hits classified by common scaffold features.

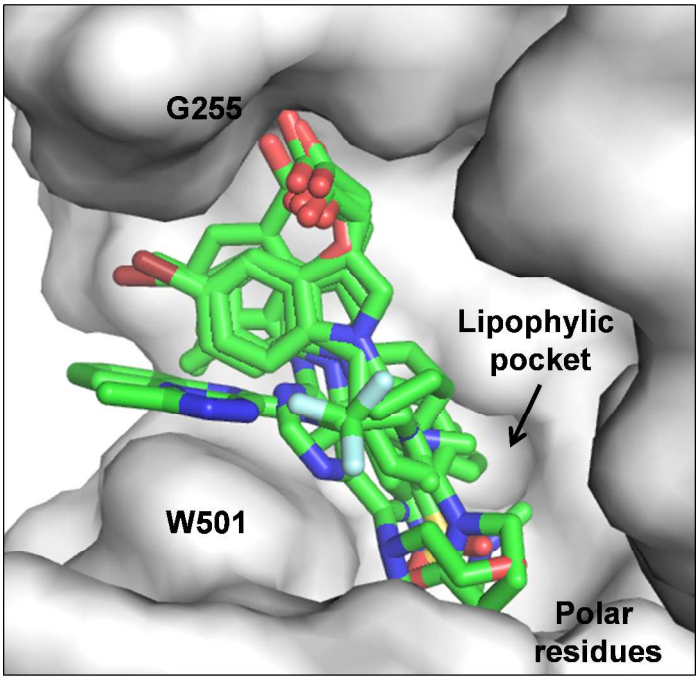

Figure 5. Shown is an overlay of twelve X-ray crystal structures of ligand-helicase complexes involving site 3+4. The ligands are derived from the five chemotype series (S1-S4, S8).

Series S2 (Indole) - Detection and Explorations. Series S2 was identified using STD NMR as a primary screen of our in-house fragment library. The library comprised ~1000 carefully-selected, small fragments (MW < 300) that are highly soluble and triaged to avoid self-aggregating compounds. The screen consisted of the preparation of samples that each comprised a mixture of three fragments at 300 μM each and HCV helicase at 3.5 μM. NMR experiments were then run for each sample where a 1D ^{1}H NMR spectrum was acquired along with a 1D STD-NMR spectrum. The 1D ^{1}H NMR spectrum provided detection of potential solubility issues and identification of diagnostic proton resonances for each fragment. The presence of signals in the STD experiment indicated that one or more of the fragments experienced binding to helicase. The samples that gave rise to STD signals were then subjected to followed-up deconvolution experiments where single compound studies identified which of the three

fragments from hit sets bound to helicase. Figure 7B shows the 1D ^{1}H reference spectrum (red) for fragment **1**, and Figure 7C displays the signals produced in the STD spectrum which confirms that fragment **1** indeed binds to helicase. Fragment 1 was analogous to similar compounds known in the literature.[13c]

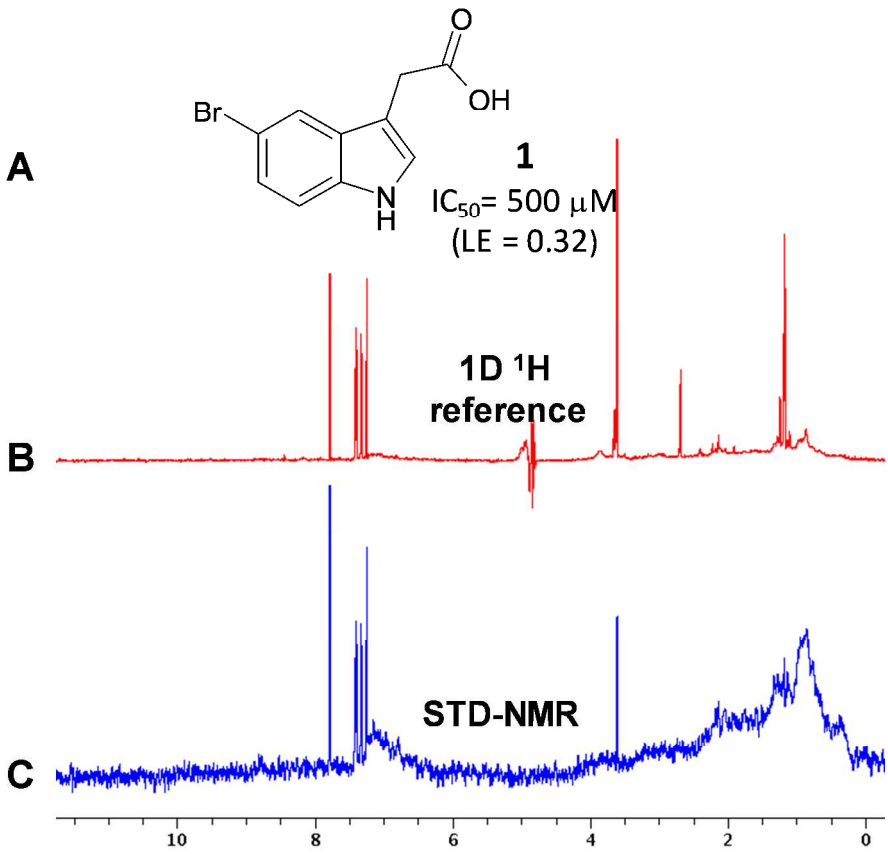

Figure 7. Identification of indole fragment by STD-NMR (A) Fragment binder **1**. (B) 1D ^{1}H NMR reference spectrum of fragment **1**. (C) Fragment **1** was discovered by STD-NMR signals (bottom spectrum in blue). The samples for STD experiments consisted of a total volume of 500 μL in deuterated buffer containing 20 mM deuterated Bis-Tris, pH 6.5, 30 mM NaCl, and 1 mM deuterated DTT.

NMR binding and competition experiments were then employed to assess binding of compound **1** specifically to site 3+4. Figure 8A shows that the sharp and intense peak of free **1** (1) broadened and shifted upon addition and binding to helicase (2). Addition of the literature

compound **2** known to bind to site 3+4 (see Figure 8),[13c] resulted in the displacement of compound **1** from the binding pocket and resonances resembling those of the original free state.

This was then corroborated by the crystal structure of **1** which showed that it indeed bound to site 3+4 (Figure 8B). It also revealed that the binding mode of the fragment was similar to that of **2** where the carboxylic acid hydrogen bonded to G255 and T269 residues. A comparison of Figure 8B and 8C suggested that a substituent growth vector from the nitrogen position toward the lipophilic pocket could provide additional interactions and potency. To this end, multiple analogues of **2** were made but without significant improvements in potency. Before further evaluating this indole series of compounds, additional NMR studies were performed to better understand the solution binding mode for control purposes.

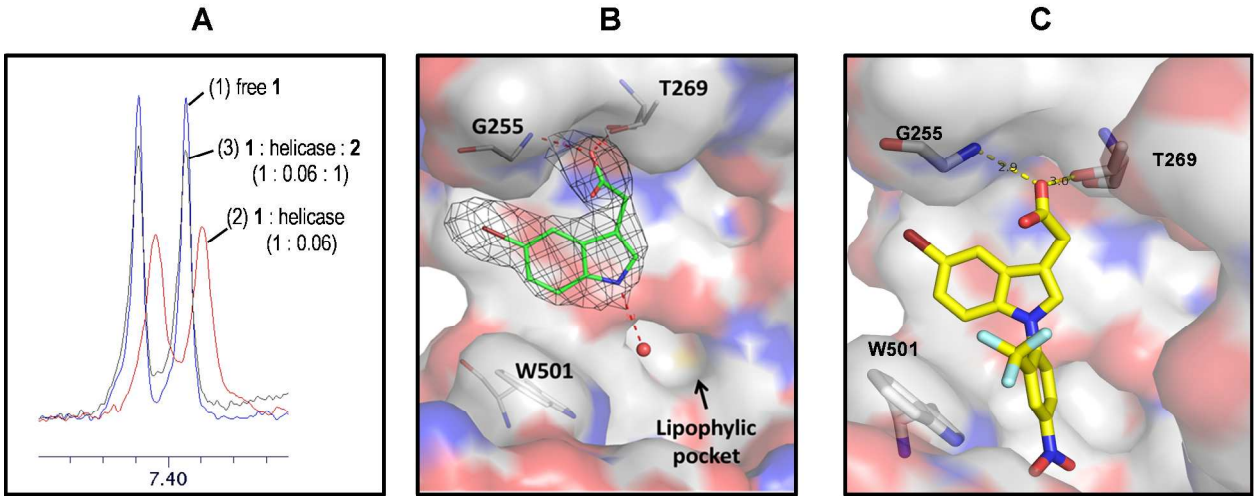

Figure 8. Characterization of Indole fragments by NMR and X-ray crystallography. (A) ^{1}H NMR binding and competition experiments - (1) 1H NMR of a resonance of free compound **1**; (2) Compound **1** in the presence of helicase; Compound **1** in the presence of helicase and compound **2**. (B) X-ray structure of compound **2** bound to site 3+4 of helicase. (C) Compound **1** bound to site 3+4 of helicase.

Direct binding of **2** to helicase was verified by the methyl-shift NMR assay as shown in Figure 9B. Methyl resonances changed positions upon the addition **2**. Also, ^{15}N TROSY experiments (Figure 9D) showed that many resonance peaks of apo helicase shifted positions upon the binding of compound **2** (blue versus red peaks of the complex) and formed a stable complex. In comparison, the Supporting Information shows an example of an unstable complex involving compound **3** from the S4 chemotype series. Thus, both NMR experiments clearly confirmed that compound **2** bound to helicase in solution.

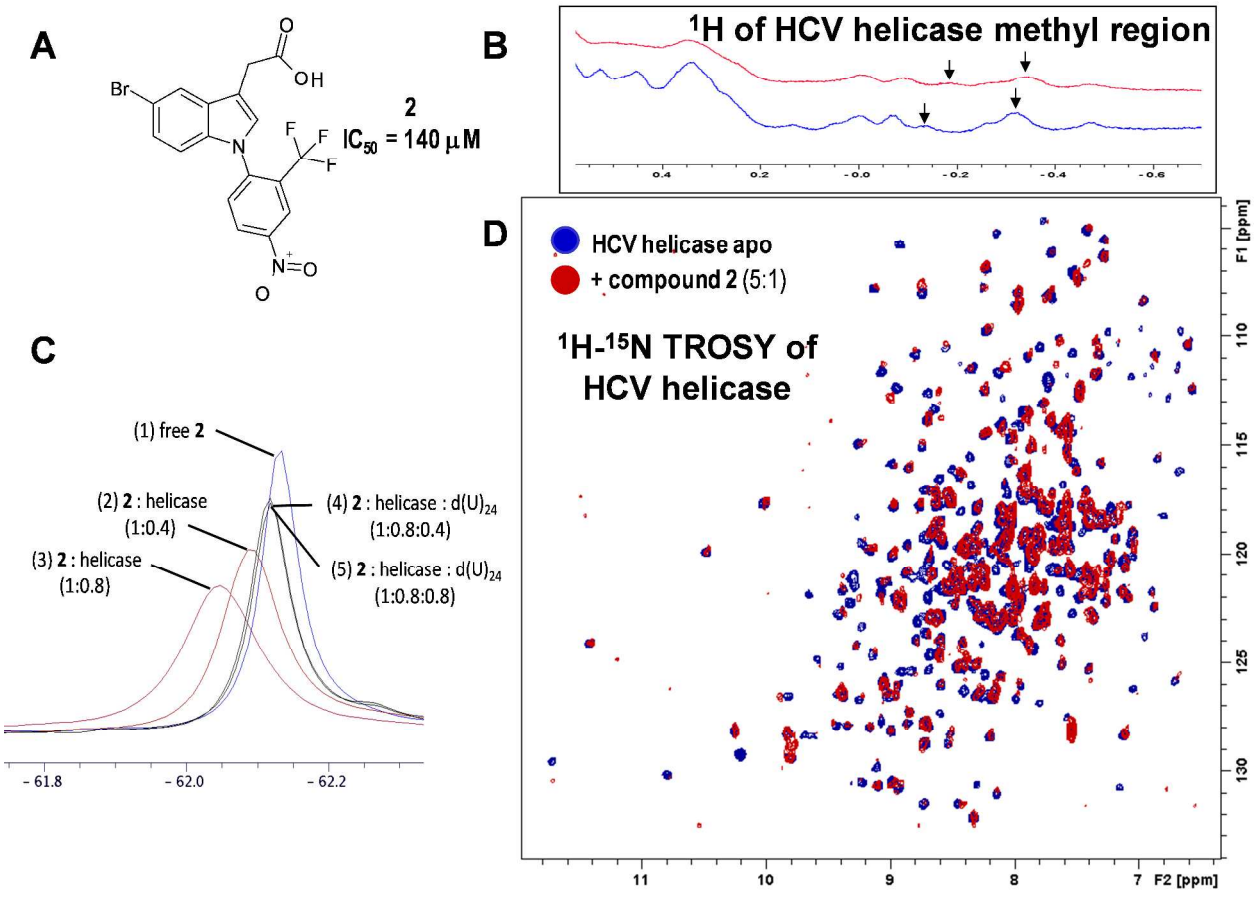

Figure 9. Characterization of tool compound **2**. (A) The primary structure and activity of compound **2**. (B) ^{1}H NMR methyl region of apo helicase (blue) and complex with compound **2** (red). (C) ^{19}F NMR spectra, - (1) resonance of free compound **2**. (2 and 3) resonance of compound **2** after adding helicase. (4 and 5) Resonance of compound **2** after adding helicase then $d(U)_{24}$. (D) ^{1}H-^{15}N TROSY of apo HCV helicase (blue) and complex with **2** (red, 1:5 ratio of helicase to ligand).

The presence of fluorine atoms on **2** also allowed for ^{19}F NMR experiments to determine if **2** was competitive with binding of a substrate, as anticipated for inhibitors of site 3+4 (see bound nucleic acid octamer in Figure 1). These experiments are shown in Figure 9C where an intense and sharp ^{19}F NMR resonance was noted for free compound **2** (blue, (1)), which then broadened and shifted upfield (left) when helicase was incrementally added, (red resonances (2) and (3)). The shift was reversible, although not completely, when the substrate mimic $d(U)_{24}$ was subsequently added (see the black resonances (4) and (5)). Thus, these studies were consistent with the desired binding properties, which improved the attractiveness of the indole series for further medicinal chemistry efforts.

Exploratory medicinal chemistry efforts focused on the initial hit **1** as the starting scaffold. Changes to this scaffold by removing the bromine atom from position 5 of compound **1** resulted in an equipotent compound (Table 1, **4**, entry 1), and it also fortuitously brought about a re-orientation of the indole. This subsequently allowed N-substitutions with better access to the lipophilic pocket, while also maintaining the carboxylic acid interactions with G255 and T269 amino acid residues (Figure 10A). Addition of a benzyl substituent **(**Table 1**, 5,** entry 2) gave a compound with 2-fold improved potency. This slight improvement could be the result from favorable π-π stacking with Trp501 or general van der walls interactions. Further substitution at position 3 of the phenyl ring was then used to target the lipophilic pocket adjacent to Trp501. The resultant SAR suggested that large lipophilic groups were preferred such that $CH_3 < Cl < I <$ alkynyl (Table 1, entries 3-6, **6-9**), consistent with the lipophilic nature of the pocket. Indeed, the crystal structure complexes of **7** and **9** showed favorable access to the pocket with increased

VDW contact with residues T298, L301, C494 and Y501, lining the pocket wall (Figure 10A and B). X-ray co-structures also revealed the flexibility of the polar residue T298 that appears to act as a gatekeeper at the lip of the pocket (Figure 10). However, substitutions with hydrogen bond donor/acceptors targeting T298, as in hydroxyl or amine groups, led to losses in potency (Table 1, **10-11**, entry 7-8). Interestingly, incorporation of an electron withdrawing nitro group (Table 1, **12-13**, entry 9-10) resulted in improved potency. In the co-crystal structure of **13** (Figure 10C), neither the methyl ether nor the nitro groups accessed the lipophilic pocket, suggesting that the increase in potency may result from electronic effects associated with a shift of the phenyl ring and a more favorable pi-pi stacking of the inhibitor above W501.

Table 1. In vitro inhibition of HCV Helicase by indole fragment hit and analogs designed to access the lipophilic pocket in the 3+4 site

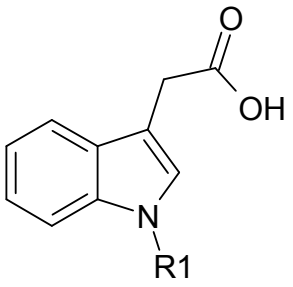

Entry	Compound	R1	Helicase IC_{50} (μM)	LE
1	**4**	H	500	
2	**5**	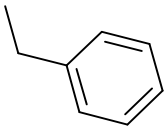	240	0.25
3	**6**	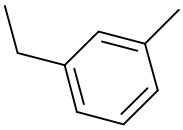	85	0.26

4	**7**	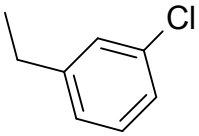	71	0.27
5	**8**	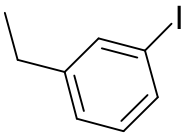	52	0.28
6	**9**	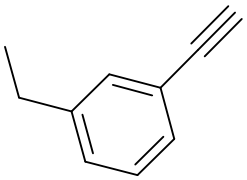	31	0.28
7	**10**	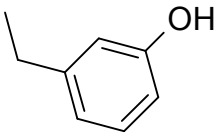	150	0.25
8	**11**	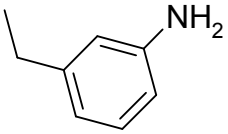	>500	NA
9	**12**	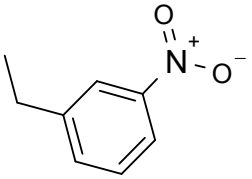	46	0.26
10	**13**	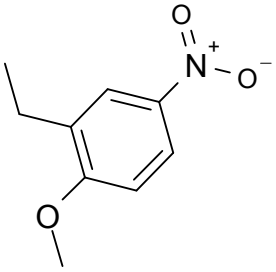	14	0.26

[a] IC_{50} values represented as μM, and averaged from a minimum of 2 determinations. Ligand Efficiency (LE) calculated by $-RT\ln(IC_{50})$ / #heavy atoms.

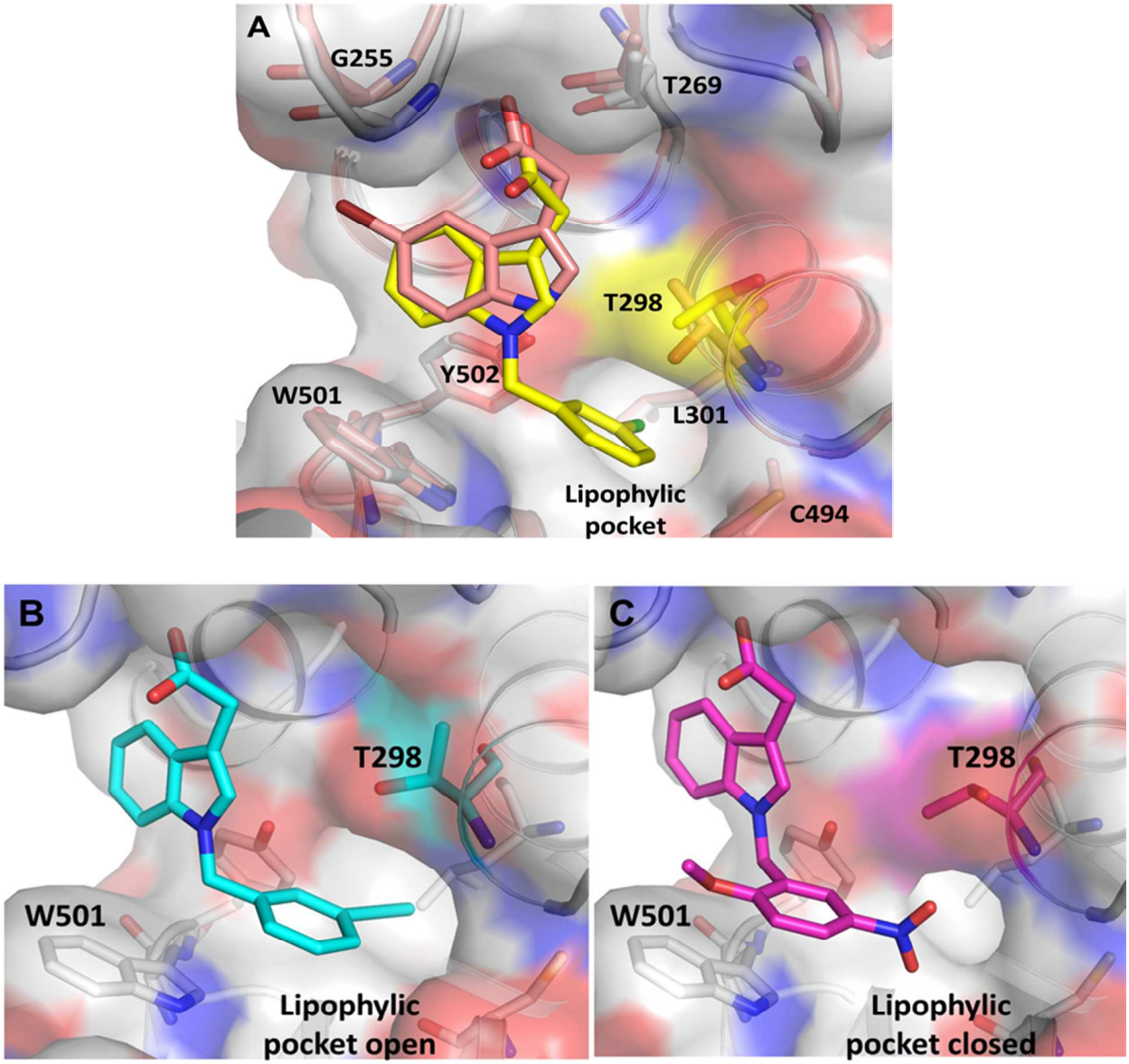

Figure 10. X-ray co-crystal structures of indole inhibitors targeting lipophilic pocket in the 3+4 site of HCV helicase. (A) Superposition of compound **1** (pink) and **7** (yellow) showing the rotation of the indole core. (B) Co-structure of compound **9.**(C) Co-structure of compound **13** showing the repositioning of the nitrophenyl ring and modulation of the lipohilic pocket size by conformational change in the gate-keeper residue T298 .

Based on fragment **7**, further optimization was then pursued at the 6-position of the indole scaffold (Table 2). Halogen substitution such as chlorine and bromine was tolerated (Table 2, **14-15**, entries 1-2), and incorporation of phenyl or 5-nitro phenylamine led to a two-

fold loss in potency (Table 2, **16-17**, entries 3-4). Substituting 3,5-diamino phenyl targeting W501 and also described in the literature, [13c] led to a significant improvement in potency (Table 2, **18**, entry 5). Combining the right-hand side of **13** with **18** led to hybrid molecule **19** (Table 2, entry 6), the most potent compound in this series. The co-crystal structure of **19** (Figure 8) shows a good overlay of the core and the phenyl diamino group is projected into solvent with one of the amines donating a hydrogen bond to the backbone carbonyl of Trp501. Interestingly, the 2-methoxy-5-nitro benzene moiety of **19** binds closer to the lipophilic pocket compared to **13**, while maintaining the π-π interaction with W501 (Figure 11B). However, the potency gain came at the expense of installing larger groups as reflected by a lower LE. Nonetheless, it was encouraging that this substitution rendered compounds **19** to be more specific. The activity window between the HCV helicase assay and the unrelated helicase A assay was 36-fold. However, the aniline substituent present on compound **19** would need to be replaced given mutagenic considerations. In conclusion, these studies suggested that the S2 indole series could serve as a starting point for further optimization. As a representative of this series, compound **19** was subjected to further biophysical characterization as discussed in the next section.

Table 2. In vitro inhibition of HCV Helicase by elaborated indole analogs.

Entry	Compound	Structure	Helicase IC50 (μM)	LE
1	**14**	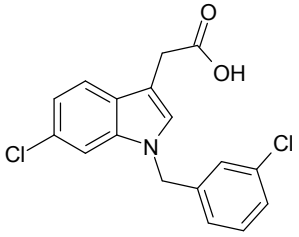	94	0.25

2	**15**	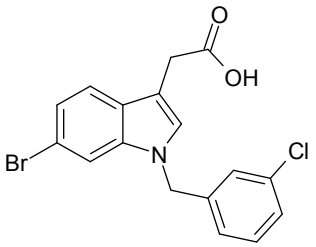	94	0.25
3	**16**	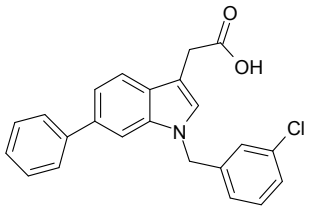	140	0.19
4	**17**	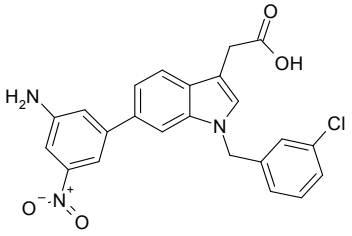	140	0.17
5	**18**	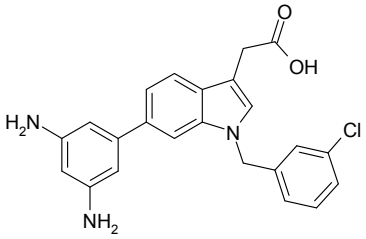	35	0.21
6	**19**	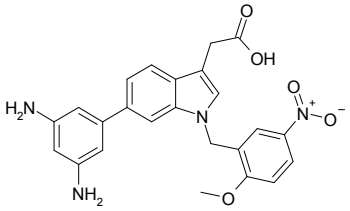	3	0.23

[a] IC_{50} values represented as μM, and averaged from a minimum of 2 determinations. Ligand Efficiency (LE) calculated by -RTln(IC_{50}) / #heavy atoms.

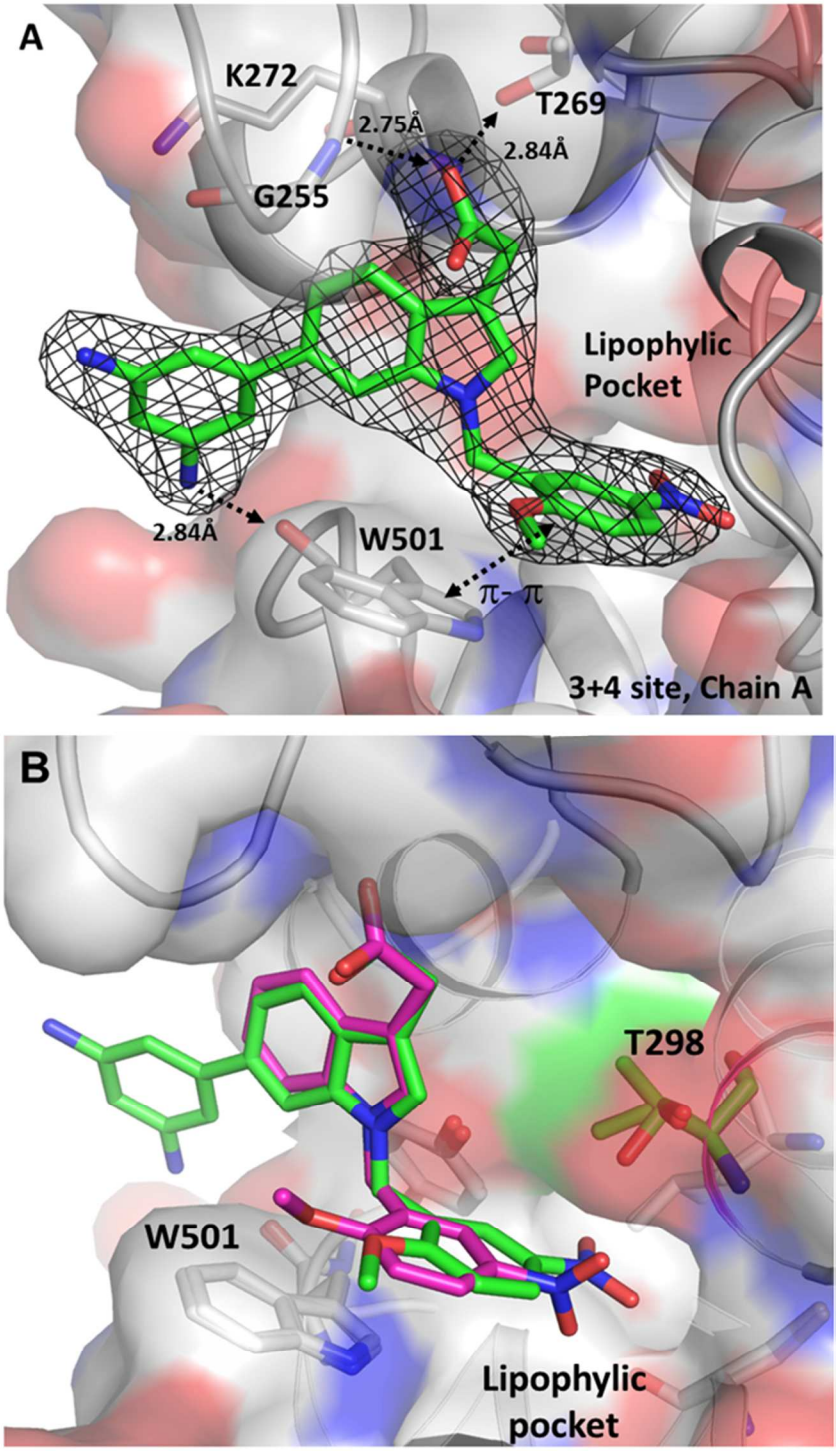

Figure 11. Binding mode of series S2 inhibitors in site 3+4 of HCV helicase. (A) The electron-density map of compound **19** bound to HCV helicase shown in stick representation (green), with molecular interactions depicted as dotted lines. The 2*Fo* - *Fc* electron-density map calculated using the ligand fit model and is represented as a mesh colored in black at a contour level of 1.0σ. (B) Superposition of co-structures of compound **13** (magenta) and **19** (green)**.**

Biophysical Characterization and Binding Kinetics for Compound 19 - K_d Determinations. To determine whether the IC_{50} values from the unwinding assays were representative of true binding affinities of inhibitors to HCV helicase, we sought to quantify the binding of a representative compound, **19**, by one or more biophysical methods that did not require immobilization of the protein. For this purpose, NMR was used to analyze the methyl region of the helicase. Figure 12B shows two helicase resonances in the methyl signature region that changed following incremental additions of inhibitor **19**. This was plotted in Figure 9A where the shift changes (Hz) versus compound concentration were fit using Graphpad (one-site binding), and K_d's of 32 and 28 μM (+/- 8) were determined. These values differ by ~10-fold from the IC_{50} values determined in the enzymatic assay (Table 2). However, NMR spectra of helicase in two different buffers (at pH 7.5 and 6.5) showed significant differences in resonance positions suggesting that structural or dynamic differences existed (Supporting Information).

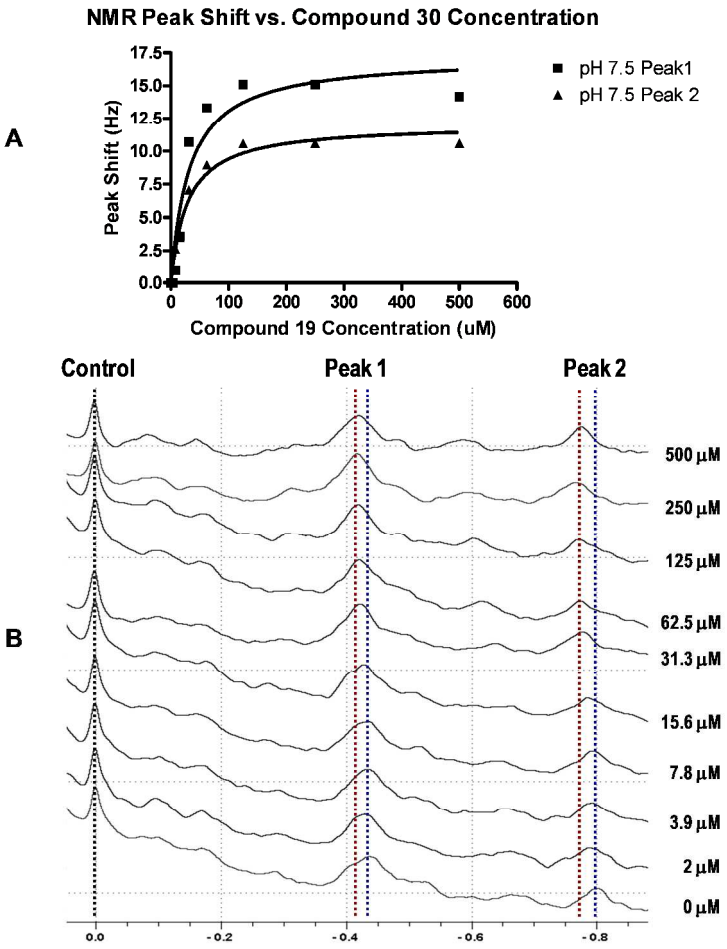

Figure 12. K_d by NMR for compound **19** binding to unlabeled HCV helicase. The ^{1}H NMR methyl region of HCV helicase is shown as a function of compound concentration. The solutions consisted of 23 µM HCV helicase GT-1a, 25 mM Tris-HCl (deuterated), pH 7.5, 5 mM MgCl2, 0.5 mM DTT (deuterated), 3% glycerol (deuterated), 1 mM EDTA (deuterated), 300 mM NaCl, 0.01% IGEPAL, 5% DMSO (deuterated).

Independently, an isothermal titration calorimetry (ITC) experiment also showed binding of compound **19** to HCV helicase, though with a K_d value (33 µM) that was also ten-fold higher than IC_{50} value from the unwinding assay (Figure 13). To achieve sufficient signal in ITC, the protein needed to be at very high concentrations, and in this case buffer components and pH had to be adjusted to achieve the required concentration. We therefore sought to identify a different biophysical technique which would require lower protein concentrations in two different buffers.

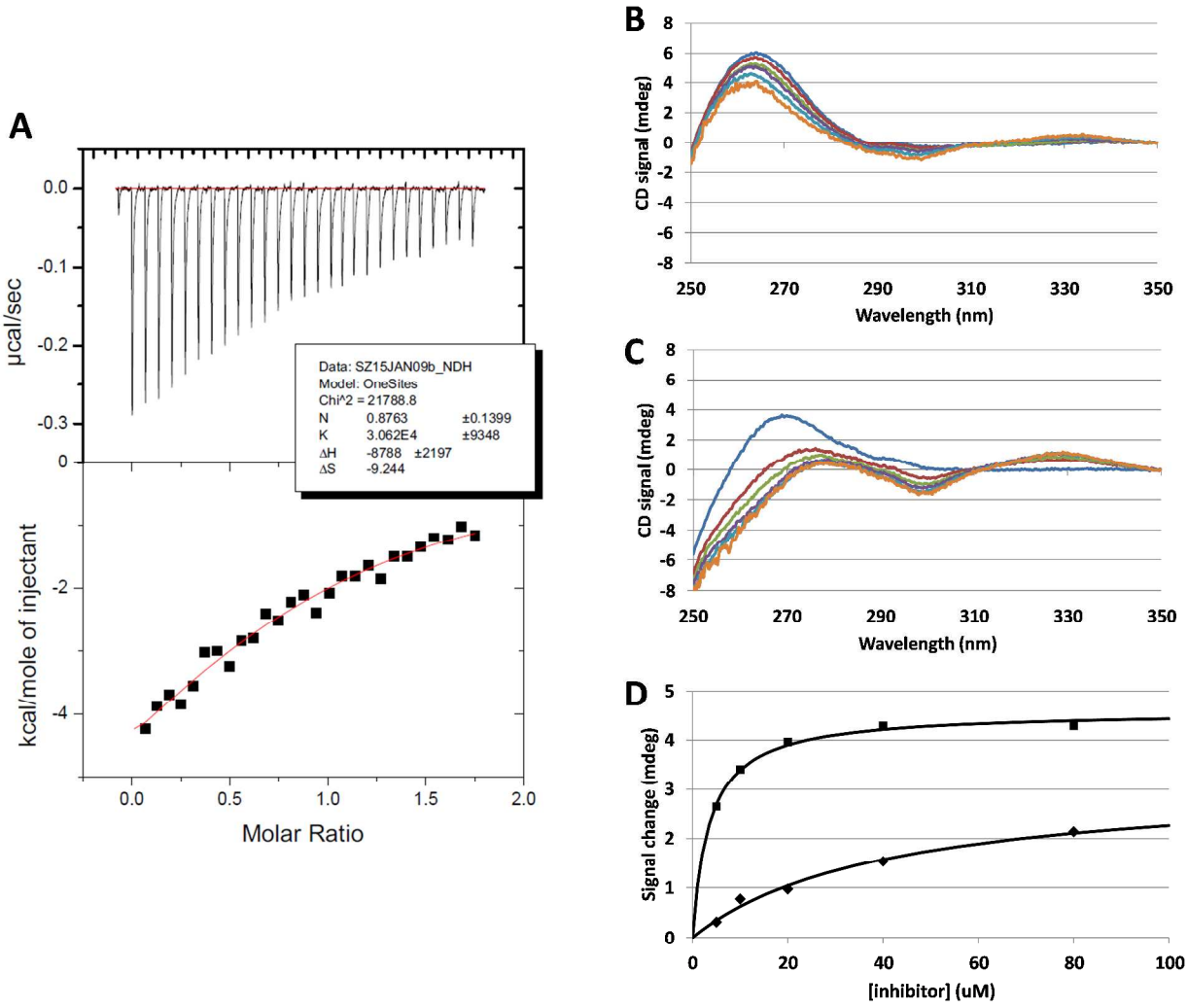

Figure 13. Thermodynamic and structural characterization of inhibitor **19**. (A) Determination of the affinity of inhibitor **19** for the HCV helicase domain by calorimetry. Top: raw data obtained at 25°C for injections of inhibitor x (300 µM) into the sample cell containing HCV helicase (35 µM). Bottom: calculated enthalpies (squares) after subtraction of the heat of dilution as determined by the later injections. Data were fit to a simple one binding site model to give the parameters shown in the inset. The association constant K is equivalent to a K_d value of 33 µM. (B and C) CD titration of compound **19** into helicase domain. Spectra obtained for solutions of the HCV helicase (8.6 µM) and 0 (dark blue), 5 µM (maroon), 10 µM (green), 20 µM (purple), 40 µM (turquoise), and 80 µM (orange) compound **19**. (B) Represents data obtained in pH 7.5 Tris buffer (similar to that used for ITC), (C) Represents data obtained in pH 6.5 PIPES, similar to that used for unwinding assays. (D) Plot of CD signal change vs. inhibitor concentration data at pH 7.5 (diamonds) and 6.5 (squares). Each data set was fit to a one site binding model by nonlinear regression giving K_d estimates of 41 ± 8 µM (max signal change 3.2 ± 0.3 mdeg) and 3.5 ± 0.3 µM (max signal change 4.6 ± 0.1) in pH 7.5 and 6.5 buffers, respectively. As a control,

it was noted that compound **19** had no significant effect on the CD spectrum of BSA (data not shown).

Unlike ITC's requirements for high protein concentrations, circular dichroism (CD) (Figure 13B and 13C) does not have such limitations and was used to further characterize the binding of compound **19** to HCV helicase. The CD spectrum of a protein in the near-UV region is determined by its tertiary structure in the region of aromatic amino acids.[19] It is sensitive to subtle perturbations in structure, which may be sensitive to ligand binding. Increasing concentrations of compound **19** mixed with HCV helicase caused a progressive change in the near-UV CD spectrum as shown in Figures 16B and 16C, for pH 7.5 (ITC/NMR) and pH 6.5 (assay) buffers, respectively. In fact, the K_d obtained by this method in the ITC/NMR buffer (41 ± 8 μM) at pH 7.5 was very similar to that obtained by ITC and NMR, and the K_d obtained in pH 6.5 assay buffer (3.5 ± 0.3 μM) was very close to that obtained in the unwinding assay. Taken together, the NMR differences noted for helicase in different buffers (Supporting Information) are consistent with the differences in determined K_d values by CD. These results help to demonstrated that the IC_{50} values measured in enzymatic assays accurately reflected the affinity of compounds for the HCV helicase domain.

CONCLUSIONS

Despite the limited success reported so far in identifying specific lead inhibitors of HCV helicase, our results suggest that this essential antiviral target may be druggable. In this work, we screened fragments and compounds from multiple sources and evaluated hits by stringent biophysical and crystallographic methods. Indole compounds from series S2 can be considered as starting points suitable for further potency improvements and cell-culture activity in replicon

assays. This series clearly binds at the more conserved 3+4 site, but it may be noteworthy that the pocket is wide and groove-like and there is an inherent flexibility of the protein in this region. To determine if the latter influences the intrinsic ligand-binding energy, one may consider acquiring a better understanding of the complementarity of the conformation and dynamics of the ligands with the helicase receptor in the free and bound states. It is conceivable that the indole series is one of the best chemotypes for this complementarity given that numerous pharmaceutical companies have screened their collections, and indole-based compounds have received the most attention.

EXPERIMENTAL SECTION

Chemistry. Compounds **2** and **3** were prepared as previously described.[13c] Compounds **1**, **4** and **6**, were purchased from commercial vendors and used directly without further purification. Preparations of fully elaborated compounds **5-7**, and **10-12** are shown in Scheme 1. The indole acetic acid was alkylated with the corresponding benzyl bromides under basic conditions to afford elaborated indoles **5-7** and **13-12**. The synthesis of analogues **8** and **9** are shown in Scheme 2. Indole ester was alkylated with 2-iodobenzylbrominde to afford the intermediate iodide. This iodide was saponified to afford the corresponding acid **8**. Alternatively prior to saponification the iodide was subjected to Sonogasheria coupling conditions (cat. Pd, Base), and TMS-acetylene to afford the coupled acetylide **9**, that was treated with stoichiometric amounts of fluoride followed by LiOH hydrolysis to afford acid **9**.

The synthesis of analogs **14** and **15** are shown in Scheme 3. 5-Bromor or chloro indole was coupled with 3-chloro benzylbromide to afford intermediates **12-13** that were subsequently saponified to the corresponding acids **14-15** under basic conditions.

The synthesis of analogs **16-19** are shown in Scheme 3. Intermediate bromide **13** was coupled with either phenylboronic acid or 3amino,5 nitrophenylboronic acid under Suzuki conditions to afford intermediated **16** and **17**. The resulting esters were saponified under mild basic conditions to afford **18** and **19**. Nitroaryl **19** was further reduced with zinc to afford bis-aniline **20**.

The synthesis of analog **19** is shown in Scheme 3. Bromoindole was treated with 2-methoxy, 5-nitrobenzyl bromide under mild basic conditions to afford intermediate **21** that was coupled under Suzuki conditions with 3,5 diaminophneylboronic acid. The resulting biaryl ester was saponified under middle basic conditions to afford analog **23**.

Chemistry General Remarks. Starting materials were obtained from commercial suppliers and used without further purification unless otherwise stated. ^{1}H NMR spectra were recorded on a Bruker UltraShield spectrometer operating at 400 MHz in solvents, as noted. Proton coupling constants (*J*) are rounded to the nearest Hz. All coupling constants are reported in hertz (Hz), and multiplicities are labeled s (singlet), bs, (broad singlet), d (doublet), t (triplet), q (quartet), dd (doublet of doublets), dt (doublet of triplets), and m (multiplet). All NMR spectra were referenced to tetramethylsilane (TMS δH 0, δC 0). All solvents were HPLC grade or higher. The reactions were followed by TLC on precoated Uniplate silica gel plates purchased from Analtech. The developed plates were visualized using 254 nm UV illumination or by PMA stain. Flash column chromatography on silica gel was performed on Redi Sep prepacked disposable silica gel columns using an Isco Combiflash, Biotage SP1 or on traditional gravity columns. Reactions were carried out under an atmosphere of argon at room temperature, unless otherwise

noted. Mass spectrometry data were obtained using the Micromass Platform LCZ (flow injection). Purity for all final compounds was >95%, and purity was evaluated by the following:

System 1: analytical HPLC using a Varian Dynamax SD-200 pump coupled to a Varian Dynamax UV-1 detector. Solvents: (A) water + 0.05% TFA and (B) acetonitrile + 0.05% TFA, flow 1.2 mL/min. Column: Vydac RP-18, 5 m, 250 mm × 4.6 mm. Photodiode array detector at 220 nm. Gradient: from 95% to 20% solvent A over 25 min.

System 2: HP 1110 Agilent LCMS using a quaternary G1311A pump coupled to a Micromass Platform LCZ detector. Solvents: (A) water + 0.1% formic acid and (B) acetonitrile + 0.1% formic acid, flow 1.5 mL/min. Photodiode array detector at 190 or 400 nm. (a) Agilent Zorbax Eclipse XDB-C8 5 μm, 4.6 mm × 150 mm column, 4.6 mm × 30 mm, 3.5 μm, from 99% to 5% solvent A over 10 min or (b) Column Agilent Zorbax C18 SB 3.5 μm, 4.6 mm × 30 mm cartridge, from 95% to 5% solvent A over 2.5 min.

Scheme 1.

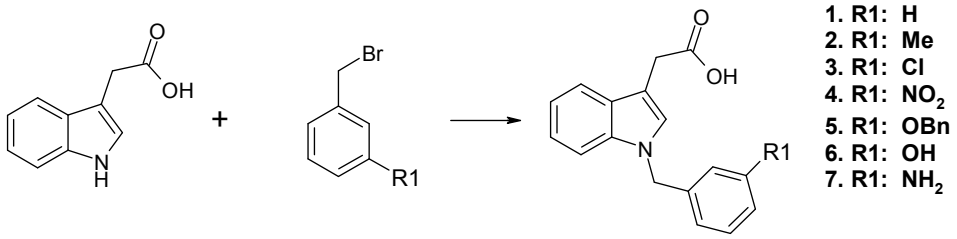

1. R1: H
2. R1: Me
3. R1: Cl
4. R1: NO_2
5. R1: OBn
6. R1: OH
7. R1: NH_2

(1-Benzyl-1H-indol-3-yl)-acetic acid (1). Sodium hydride (55 mg, 1.4 mmol) was suspended in DMF (4 mL) and to cooled to 0 ^{0}C in an ice-water bath. Indole-3-acetic acid (80 mg. 0.45 mmol) was added and the resulting slurry stirred at 0 ^{0}C for 30 minutes. Benzyl bromide (93 mg, 0.55 mmol) was added and the reaction warmed to room temperature for 1 h. The reaction mixture was quenched with water, and the solvent evaporated in vacuo. The crude mixture purified by reverse phase HPLC to afford **1** (25 mg, 21 %).LCMS (ES+) *m*/*z* found 266;

retention time 0.88 min. HPLC, retention time 13.8 min.^{1}H NMR (400 MHz, DMSO-d_6) δ 12.13 (br. s., 1H), 7.44 (d, *J*=7.86 Hz, 1H), 7.35 (d, *J*=8.20 Hz, 1H), 7.32 (s, 1H), 7.20-7.26 (m, 2H), 7.16-7.19 (m, 1H), 7.11-7.15 (m, 2H), 7.03 (t, *J*=7.50 Hz, 1H), 6.94 (t, *J*=7.50 Hz, 1H), 5.31 (s, 2H), 3.58 (s, 2H).

[1-(3-Methyl-benzyl)-1H-indol-3-yl]-acetic acid (2). Sodium hydride (55 mg, 1.4 mmol) was suspended in DMF (4 mL) and to cooled to 0 ^{0}C in an ice-water bath. Indole-3-acetic acid (80 mg. 0.45 mmol) was added and the resulting slurry stirred at 0 ^{0}C for 30 minutes. 3-Methylbenzyl bromide (101 mg, 0.55 mmol) was added and the reaction warmed to room temperature for 1 h. The reaction mixture was quenched with water, and the solvent evaporated in vacuo. The crude mixture purified by reverse phase HPLC to afford **2** (92 mg, 72 %). LCMS (ES+) *m*/*z* found 280; retention time 0.94 min. HPLC, retention time 14.5 min.^{1}H NMR (400 MHz, DMSO-d_6) δ 12.21 (s, 1H), 7.51 (d, *J*=7.83 Hz, 1H), 7.42 (d, *J*=8.08 Hz, 1H), 7.31-7.40 (m, 1H), 7.18 (t, *J*=7.33 Hz, 1H), 6.88-7.14 (m, 2H), 5.33 (s, 2H), 3.65 (s, 2H), 2.24 (s, 3H).

[1-(3-Chloro-benzyl)-1H-indol-3-yl]-acetic acid (3). Sodium hydride (3.4 g, 85.6 mmol) was suspended in DMF (40 mL) and cooled to 0 ^{0}C in an ice-water bath. Indole-3-acetic acid (5 g. 28.5 mmol) in DMF (40 mL) was added and the resulting slurry stirred at 0 ^{0}C for 30 minutes. 3-Chlorobenzyl bromide (4.5 mL, 34.3 mmol) is added and the reaction allowed to warm to room temperature. The reaction was quenched with 1 N HCl, and extracted with EtOAc three times. The combined organic layers were washed with water, then brine and evaporated in vacuo. The crude product was purified on silica (EtOAc/Hexane) to afford **3** (7.4 g 86%). LCMS (ES+) *m*/*z* found 300; retention time 0.94 min. HPLC, retention time 14.6 min.^{1}H NMR (400 MHz, DMSO-d_6) δ 12.20 (br. s., 1H), 7.52 (d, *J*=8.28 Hz, 1H), 7.43 (d, *J*=8.28 Hz, 1H), 7.41 (s, 1H), 7.27-7.36 (m, 2H), 7.25 (s, 1H), 7.07-7.17 (m, 2H), 6.99-7.04 (m, 1H), 5.40 (s, 2H), 3.66 (s, 2H).

[1-(3-Nitro-benzyl)-1H-indol-3-yl]-acetic acid (4). To Indole-3-acetic acid (50 mg, 0.29 mmol) in DMF (1 mL) was added 3-nitrobenzylbenzyl bromide (76 mg, 0.35 mmol) followed by NaHMDS (0.44 mL, 0.87 mmol). The resulting slurry was stirred at room temperature for 2 hours. The reaction mixture was quenched with water, and the solvent evaporated in vacuo. The crude mixture was purified by reverse phase HPLC to afford **4** (2 mg, 3 %). LCMS (ES+) *m*/*z* found 311; retention time 0.85 min. HPLC, retention time 13.5 min.^{1}H NMR (400 MHz, DMSO-d_6) δ 12.21 (s, 1H), 7.97-8.21 (m, 2H), 7.57-7.64 (m, 2H), 7.53 (d, *J*=7.78 Hz, 1H), 7.46 (s, 1H), 7.45 (d, *J*=7.80 Hz, 2H), 7.11 (t, *J*=7.30 Hz, 1H), 7.03 (t, *J*=7.30 Hz, 1H), 5.55 (s, 2H), 3.67 (s, 2H).

[1-(3-Hydroxy-benzyl)-1H-indol-3-yl]-acetic acid (6). Sodium hydride (132 mg, 3.3 mmol) suspended in DMF (3 mL) and to cooled to 0 ^{0}C in an ice-water bath. Indole-3-acetic acid (175 mg. 1.0 mmol) was added and the resulting slurry stirred at 0 ^{0} C for 30 minutes. 1-Benzyloxy-3-bromomethyl-benzene (320 mg, 1.2 mmol) was added and the reaction warmed to room temperature for 1 h. The reaction mixture was quenched with water, and the solvent was evaporated in vacuo. The crude mixture purified by reverse phase HPLC to afford **5** (371 mg, 99 %). **5** (295 mg, 0.79 mmol) was suspended in MeOH/EtOAc (6 mL/6 mL) and 10% Pd/C (85 mg, 0.079 mmol)was added in one portion. The system was purged with H_2 gas three times, and stirred at room temperature for 4 hour under an atmosphere of hydrogen gas. Upon completion the reaction mixture was filtered through celite and was washed with MeOH and EtOAc. The solvent was evaporated in vacuo, and the crude mixture purified by reverse phase HPLC to afford **6** (116 mg, 52 %). LCMS (ES+) *m*/*z* found 282; retention time 0.73 min. HPLC, retention time 11.9 min.^{1}H NMR (400 MHz, DMSO-d_6) δ 12.01 (br. s, 1H), 9.35 (br. s, 1H), 7.51

(d, *J*=7.83 Hz, 1H), 7.38 (d, *J*=8.22 Hz, 1H), 7.34 (s, 1H), 7.04-7.14 (m, 2H), 7.00 (t, *J*=7.50 Hz, 1H), 6.58-6.66 (m, 2H), 6.53 (t, *J*=1.70 Hz, 1H), 5.28 (s, 2H), 3.65 (s, 2H).

[1-(3-Amino-benzyl)-1H-indol-3-yl]-acetic acid (7). [1-(3-Nitro-benzyl)-1H-indol-3-yl]-acetic acid (**4**) (200mg, 0.65 mmol) was suspended in MeOH/EtOAc (6 mL/6 mL) and 10% Pd/C (103mg, 0.097 mmol) was added in one portion. The system was purged with H_2 gas three times, and stirred at room temperature for 4 hours under an atmosphere of hydrogen gas. Upon completion, the reaction mixture was filtered through celite, washed with MeOH and EtOAc, and evaporated in vacuo. The crude mixture was purified by reverse phase HPLC to afford **7** (151 mg, 84 %). LCMS (ES+) *m*/*z* found 281; retention time 0.60 min. HPLC, retention time 8.8 min.^{1}H NMR (400 MHz, DMSO-d_6) δ 12.22 (br. s, 2H), 8.57 (br. s, 3H), 7.53 (d, *J*=7.84 Hz, 1H), 7.35-7.42 (m, 2H), 7.27 (t, *J*=7.79 Hz, 1H), 7.10 (t, *J*=7.30 Hz, 1H), 7.02 (t, *J*=7.60 Hz, 1H), 6.98 (d, *J*=7.60 Hz, 1H), 6.94 (d, *J*=7.60 Hz, 1H), 5.37 (s, 2H), 3.66 (s, 2H).

Scheme 2. [1-(3-Ethynyl-benzyl)-1H-indol-3-yl]-acetic acid (11)

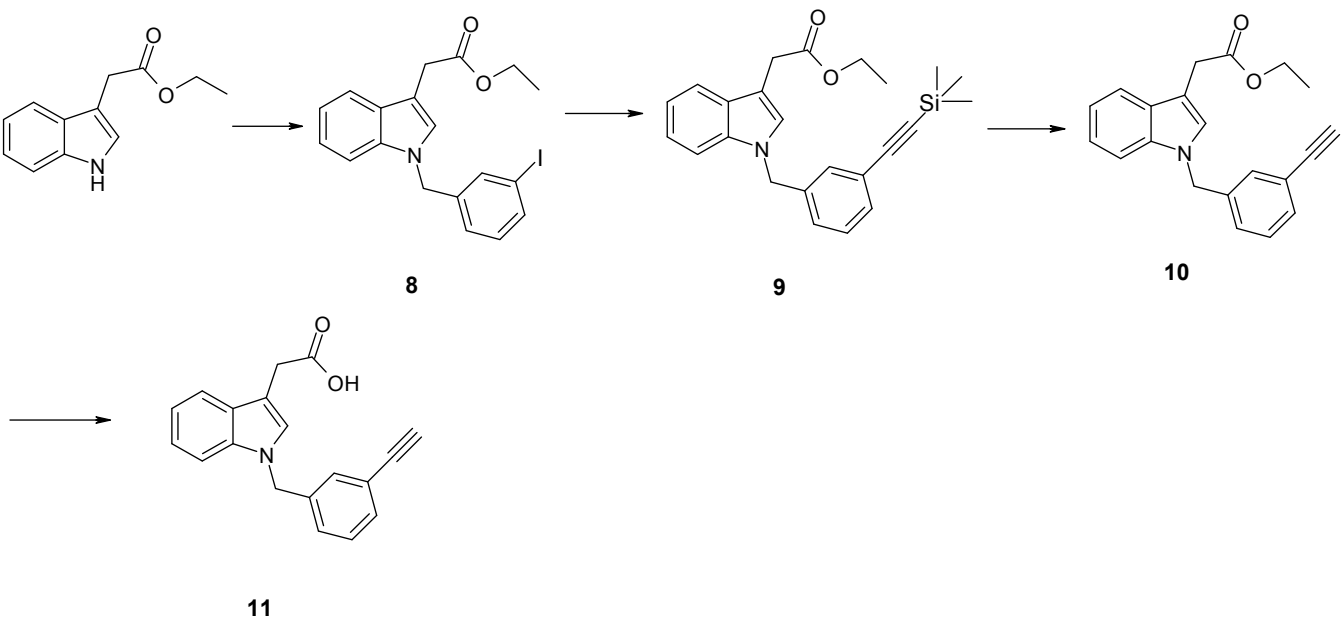

8 **9** **10**

11

Sodium hydride (173 mg, 4.3 mmol) was suspended in DMF (20mL) and cooled to 0 °C in an ice-water bath. Ethyl Indole-3-acetate (800 mg, 3.9 mmol) was added and the resulting slurry stirred at 0 °C for 30 minutes. 3-Iodobenzyl bromide (1.4 g, 4.7 mmol) was added and the reaction allowed to warm to room temperature. The reaction was quenched with 1 N HCl, and the solvent was evaporated in vacuo. The crude product was purified on silica (EtOAc/Hexane) to afford **8** (582 mg 35%).

A flask was charged with aryl iodide **8** (582 mg, 1.4 mmol), CuI (26 mg, 0.14 mmol) and $Pd(PPh_3)_4Cl_2$ (49 mg, 0.07 mmol) followed by degassed triethylamine (4 mL). The reaction was stirred at room temperature and TMS-acetylene (545 mg, 5.5 mmol) added dropwise over five minutes. The resulting suspension was stirred at 70 °C for 3 hours, then cooled to room temperature. The reaction was quenched with water, and extracted into EtOAc three times. The combined EtOAc was evaporated in vacuo, and the crude product purified on silica (EtOAc/Hexane) to afford **9** (499 mg, 92 %).

To a solution of **9** (499 mg, 1.3 mmol) in THF (4 mL) was slowly added TBAF (1M in THF, 1.9 mL, 1.9 mmol). The reaction was stirred at room temperature overnight, quenched with saturated NH_4Cl and extracted into EtOAc. The solvent was evaporated in vacuo, and the crude product was purified on silica (EtOAc/Hexane) to afford **10** (335 mg, 88 %).

To a stirred solution of **10** (200 mg, 0.63 mmol) in THF (4 mL) and dioxane 4 (mL) was added 2 M NaOH (1.3 mL, 2.5 mmol). The reaction mixture was stirred at 55 °C for 4 hours. The reaction mixture was then acidified to pH 3 with 2 N HCl, and solvent was evaporated in vacuo. The crude mixture was purified by reverse phase HPLC to afford **11** (133 mg, 73 %). LCMS (ES+) *m*/*z* found 290; retention time 0.90 min. HPLC, retention time 14.2 min.^{1}H NMR (400 MHz, DMSO-d_6) δ 12.20 (br. s, 1H), 7.52 (d, *J*=7.86 Hz, 1H), 7.42 (d, *J*=8.10 Hz, 1H), 7.40 (s,

1H), 7.20-7.37 (m, 4H), 7.10 (t, *J*=7.50 Hz, 1H), 7.01 (t, *J*=7.50 Hz, 1H), 5.38 (s, 2H), 3.66 (s, 2H).

Scheme 3.

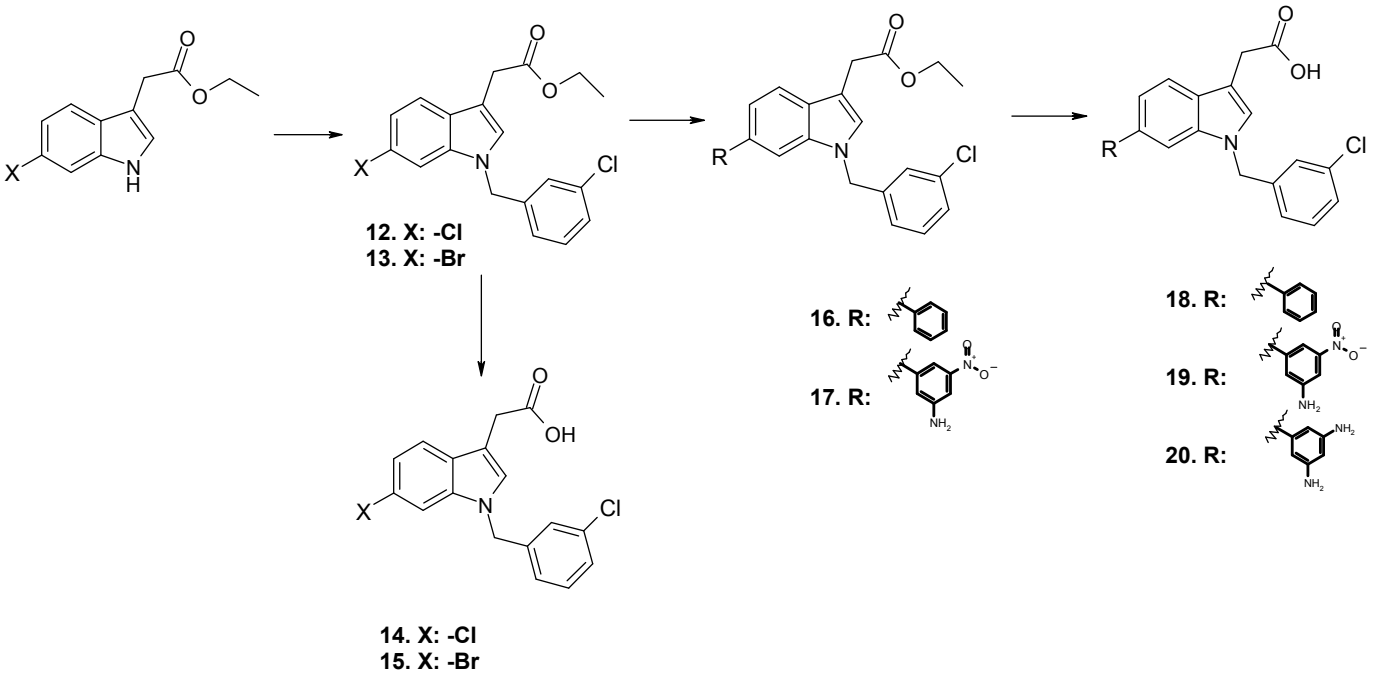

[6-Chloro-1-(3-chloro-benzyl)-1H-indol-3-yl]-acetic acid (14). (6-Chloro-1H-indol-3-yl)-acetic acid ethyl ester (300 mg, 1.3 mmol) was suspended in DMF (6 mL) and cooled to 0 °C in an ice-water bath. Potassium *tert*-butoxide (148 mg. 1.3 mmol) was added and the resulting slurry stirred at 0 °C for 20 minutes. 3-Chlorobenzyl bromide (0.17 mL, 1.3 mmol) was added and the reaction mixture stirred at room temperature for 4h. The reaction was quenched with 1 N HCl, and extracted with EtOAc. The solvent was evaporated in vacuo to give **12**.

To a stirred solution of **12** (453 mg, 1.3 mmol) in EtOH (6 mL) was added 5 N NaOH (3 mL) solution. The reaction mixture was stirred at room temperature for 1 hour. The reaction mixture was then acidified to pH 1 with 2 N HCl, and solvent was evaporated in vacuo. The crude mixture purified by reverse phase HPLC to afford **14** (210 mg, 50 %). LCMS (ES+) *m*/*z* found 334; retention time 1.02 min. HPLC, retention time 15.5 min.^{1}H NMR (400 MHz, CHLOROFORM-d) δ 7.54 (d, *J*=8.47 Hz, 1H), 7.22-7.28 (m, 2H), 7.08-7.17 (m, 3H), 6.94-6.99 (m, 1H), 5.23 (s, 2H), 3.81 (s, 2H).

[6-Bromo-1-(3-chloro-benzyl)-1H-indol-3-yl]-acetic acid (15). (6-Bromo-1H-indol-3-yl)-acetic acid ethyl ester (356 mg, 1.3 mmol) was suspended in DMF (6 mL) and cooled to 0 °C in an ice-water bath. Potassium *tert*-butoxide (148 mg. 1.3 mmol) was added and the resulting slurry stirred at 0 °C for 20 minutes. 3-Chlorobenzyl bromide (0.17 mL, 1.3 mmol) was added and the reaction mixture at room temperature for 4h. The reaction was quenched with 1 N HCl, and extracted with EtOAc. The solvent was evaporated in vacuo to give **13**.

To a stirred solution of **13** (513 mg, 1.3 mmol) in EtOH (6 mL) was added 5 N NaOH (2 mL). The reaction mixture was stirred at room temperature for 1 hour. The reaction mixture was acidified to pH 1 with 2 N HCl and the solvent was evaporated in vacuo. The crude mixture was purified by reverse phase HPLC to afford **15** (288 mg, 60 %). LCMS (ES+) *m*/*z* found 378; retention time 1.04 min. HPLC, retention time 15.7 min.^{1}H NMR (400 MHz, CHLOROFORM-d) δ 7.50 (d, *J*=8.46 Hz, 1H), 7.40 (d, *J*=1.70 Hz, 1H), 7.21-7.33 (m, 4H), 7.06-7.16 (m, 2H), 6.96 (d, *J*=7.04 Hz, 1H), 5.22 (s, 2H), 3.80 (s, 2H).

[1-(3-Chloro-benzyl)-6-phenyl-1H-indol-3-yl]-acetic acid (18). A stirred mixture of **13** (81 mg, 0.20 mmol), phenyl boronic acid (49 mg, 0.40 mmol), 2 M Na_2CO_3 solution (0.40 mL, 0.80 mmol) and $Pd(PPH_3)_4$ (23 mg, 0.02 mmol) in toluene (2mL) and EtOH (1mL)was degassed

with N_2 for 1 min and heated at 80 ^oC for 20 min in microwave reactor. The resulting mixture was diluted with EtOAc and washed with brine. The solvent was evaporated in vacuo, and the crude product purified on silica (EtOAc/Hexane) to afford **16** (76 mg, 94 %).

To a stirred solution of **16** (76 mg, 0.19 mmol) in EtOH (6 mL) was added 2 N NaOH (0.47 mL, 0.95 mmol) solution. The reaction mixture was stirred at 58 ^oC for 2 hours. The reaction mixture was acidified to pH 1 with 2 N HCl and the resulting precipitate collected and dried to give **18** (71 mg, 78%). LCMS (ES+) *m*/*z* found 376; retention time 1.1 min. HPLC, retention time 16.5 min.^{1}H NMR (400 MHz, DMSO-d_6) δ 7.75 (d, *J*=6.06 Hz, 2H), 7.72 (s, 1H), 7.69 (d, *J*=8.29 Hz, 1H), 7.50 (t, *J*=7.58 Hz, 2H), 7.30-7.44 (m, 7H), 7.23 (d, *J*=7.20 Hz, 1H), 5.51 (s, 2H), 3.44 (s, 2H).

[1-(3-Chloro-benzyl)-6-(3,5-diamino-phenyl)-1H-indol-3-yl]-acetic acid (20). A stirred mixture of **13** (200 mg, 0.49 mmol), 3-amino-5-nitrobenzeneboronic acid (179 mg, 0.95 mmol), 2 M Na_2CO_3 solution (0.98 mL, 1.9 mmol) and $Pd(PPh_3)_4$ (57 mg, 0.05 mmol) in toluene (5 mL) and EtOH (2.5 mL)was degassed with N_2 for 1 min and heated at 80 ^oC for 20 min in microwave reactor. The resulting mixture was diluted with EtOAc and washed with brine. The solvent was evaporated in vacuo and the crude product was purified on silica (EtOAc/Hexane) to afford **17** (188 mg, 82 %).

To a stirred solution of **17** (188 mg, 0.41 mmol) in THF (6 mL) and dioxane (6 ML) was added 2 N NaOH (0.81 mL, 1.6 mmol) solution. The reaction mixture was stirred at 55 ^oC for 4 hours. The reaction mixture was acidified to pH 3 with 2 N HCl and the resulting precipitate collected and dried to afford **19** (163 mg, 92 %).

19 (145 mg, 0.33 mmol) and zinc dust (640 mg, 9.8 mmol) were suspended in MeOH (7 mL) and THF (10 mL). Hydrazine (2.4 mL, 50.2 mmol) was added and the resulting mixture

stirred at room temperature under Argon for 4 hours. Solvent was evaporated in vacuo and the crude mixture purified by reverse phase HPLC to afford **20** (126 mg, 93 %). LCMS (ES+) *m*/*z* found 408; retention time 0.55 min. HPLC, retention time 10.2 min.^{1}H NMR (400 MHz, DMSO-d_6) δ 7.59-7.63 (m, 2H), 7.46 (s, 1H), 7.29-7.39 (m, 2H), 7.21-7.26 (m, 2H), 7.13 (d, *J*=7.29 Hz, 1H), 6.80 (d, *J*=1.92 Hz, 2H), 6.49 (t, *J*=1.91 Hz, 1H), 5.49 (s, 2H), 3.70 (s, 2H).

Scheme 4.

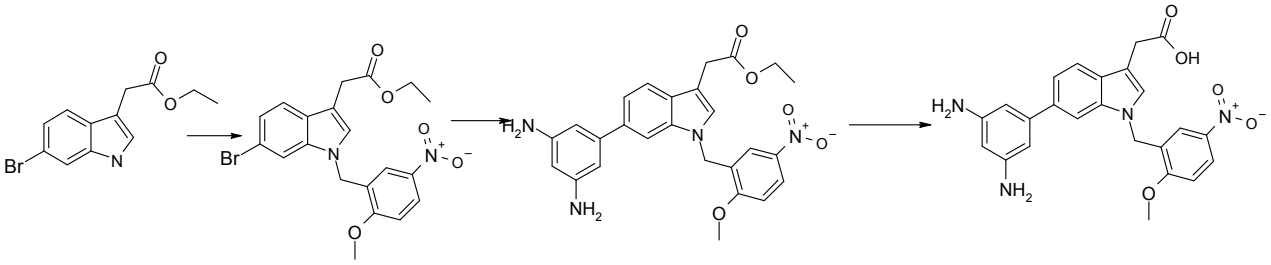

[6-(3,5-Diamino-phenyl)-1-(2-methoxy-5-nitro-benzyl)-1H-indol-3-yl]-acetic acid (23).

(6-Bromo-1H-indol-3-yl)-acetic acid ethyl ester (800 mg, 2.8 mmol) was suspended in DMF (10 mL) and cooled to 0 °C in an ice-water bath. Cesium carbonate (1.4 g. 4.3 mmol) was added and the resulting slurry stirred at 0 °C for 20 minutes. 2-Bromomethyl-1-methoxy-4-nitro-benzene (837 mg, 3.4 mmol) was added in one portion, and the reaction mixture stirred at room temperature for 2h. The reaction was quenched with saturated ammonium chloride, and extracted with EtOAc. Combined organic layer washed with water followed by brine. The solvent was evaporated in vacuo, and the crude product purified on silica (EtOAc/Hexane) to afford **21** (958 mg, 76 %).

A stirred mixture of **21** (100 mg, 0.22 mmol), 3,5-diaminophenylboronic acid (101 mg, 0.67 mmol) , 2 M Na_2CO_3 solution (0.67 mL, 1.3 mmol) and $Pd(PPH_3)_4$ (51 mg, 0.05 mmol) in toluene (2 mL) and EtOH (1 mL) was degassed with N_2 for 1 min, then heated at 80 ^oC for 20 min in microwave reactor. The resulting mixture was diluted with EtOAc and washed with brine. The solvent was evaporated in vacuo to give **22**.

To a stirred solution of **22** (104 mg, 0.22 mmol) in THF (6 mL) was added 5 N NaOH (0.44 mL, 2.2 mmol). The reaction mixture was stirred at 70 ^oC for 2 hours. The reaction mixture was acidified to pH 3 with 2 N HCl, evaporated and the crude mixture purified by reverse phase HPLC to afford **23** (16 mg, 16 %). LCMS (ES+) *m*/*z* found 447; retention time 0.49 min. HPLC, retention time 9.7 min.

^1H NMR (400 MHz, DMSO-d_6) δ 12.28 (br. s, 1H), 8.23 (dd, *J*=2.87, 9.10 Hz, 1H), 7.60-7.65 (m, 2H), 7.58 (d, *J*=1.46 Hz, 1H), 7.44 (s, 1H), 7.31 (d, *J*=9.17 Hz, 2H), 7.24 (dd, *J*=1.47, 8.29 Hz, 1H), 6.76 (s, 2H), 6.44 (s, 1H), 5.47 (s, 2H), 4.03 (s, 3H), 3.70 (s, 2H).

Expression and Purification of NS3/NS4A Protein and NS3 Helicase Domain. The full-length genotype 1b (strain HCV40) NS3/NS4A heterodimer was expressed from *E. coli* and purified as described previously.[25-26] The genotype 1a (strain H) NS3 helicase domain has been reported previously.[22] The N-terminal hexa-histidine-tagged protein was expressed from the pET 11a vector in *E.Coli* strain BL-21 (DE3). Expression was performed in BioFlo III (5 L) and BioFlo 5000 (30 L) fermenters using Circle Grow medium (Q-Biogene). The fermentor was inoculated with an overnight culture (approximately 15 mL/L) and cells allowed to grow at 37°C until reaching an OD_{600} of 6-7. Temperature was then lowered to 18°C, and IPTG was added to 1 mM. Throughout, pH was maintained at 7.0 and oxygen at 30% saturation. Cells were harvested 16-18 hours after induction, harvested by centrifugation, and then frozen at -80°C prior to

purification. Frozen cell pellets were thawed and suspended in buffer A (50 mM sodium phosphate, 500 mM NaCl, 10% glycerol, 2 mM TCEP, pH 7.8) containing protease inhibitors pepstatin, leupeptin, antipain (each at 1 μg/mL) and PMSF (1 mM). Subsequent steps were performed at 4°C. Resuspended cells were lysed by 3-4 passages through a Microfluidizer (Microfluidics), and the mixture was centrifuged at 25,000xg. The supernatant was mixed Ni-chelating Sepharose (0.2 mL/g cells), mixed gently for 30 min, then the Sepharose was loaded into a column. Remaining chromatography steps were performed with an FPLC (Pharmacia). NS3-bound Ni-sepharose was washed with 5 column volumes buffer A plus 5% buffer B (buffer A containing 500 mM imidazole), then bound proteins were eluted using a gradient from 5%-100% buffer B over 20 column volumes. NS3 helicase typically eluted at approximately 60% buffer B (verified by SDS-PAGE). Pooled fractions were diluted four-fold with buffer C (25 mM Tris/HCl, 10 mM NaCl, 10% glycerol, 1 mM TCEP, 1 mM EDTA) and applied to polyuridine Sepharose column (25 ml per 30 g of frozen cell pellet). After loading, the column was washed with buffer C and then protein was eluted using a gradient of 10 mM to 1 M NaCl. NS3 helicase typically eluted at 700 mM NaCl. The purified protein was dialyzed against 50 mM Tris-HCl, 300 mM NaCl, 10% glycerol, 0.05% dodecyl-β-D-maltoside, pH 6.8 and stored at -80°C.

The genotype 1a (strain H) NS3 helicase domain has been reported previously.[22] We expressed the N-terminal hexa-histidine-tagged protein from the pET 11a vector in *E.Coli* strain BL-21 (DE3) and purified by a Nickel column, followed by a Poly-U agarose column. The purified protein was dialyzed against 50 mM Tris-HCl, pH 6.8 (RT), 300 mM NaCl, 10% glycerol, 0.05% dodecyl-β-D-maltoside, and stored at -80°C. Human RNA helicase A, used as a counterscreen, was expressed and purified as described.[27]

Unwinding Assays. Two similar assays were used to assess the sensitivity of NS3 helicase to inhibitors. In one version, an RNA oligonucleotide duplex was unwound in the presence of genotype 1b NS3-NS4A protein. In the other, a DNA oligonucleotide duplex served as the substrate for the genotype 1a helicase domain. Both the RNA and DNA assays have been described;[28] in that study, a different protein was used, genotype 1b NS3/NS4A (strain Con1), but the protein concentrations and other conditions were the same. Briefly, the substrates consisted of a 34-mer with a Cy3 fluorophore attached at the 3' end and a 45-mer containing a black hole quencher (BHQ) group at the 5' terminus. Unwinding reactions (both RNA and DNA substrates) were performed in the presence of a 10-fold excess of ssDNA trap complementary to the Cy3 oligonucleotide. Reactions were run in 384-well plates in a volume of 20 μL per well. The assay buffer was composed of 50 mM PIPES, 2 mM TCEP, 3 mM $MgCl_2$, 2.5% DMSO, 0.0625% n-dodecyl-β-D-maltoside, 5 nM substrate, 100 μg/mL BSA, 50 nM ssDNA trap, and 2 mM ATP (pH 6.5). 0.15 U/μL RNAsin was added for assays with the RNA substrate. The NS3/NS4A protein concentration in RNA substrate reactions was 10 nM and the NS3 helicase domain concentration in DNA unwinding reactions was 15 nM. Potential inhibitors were dissolved in DMSO and diluted in buffer, then tested at either a single concentration for screening or in serial two-fold dilutions. Reactions were run for one hour at room temperature (approximately 23°C), and then fluorescence was measured using a VictorII multi-mode plate reader (Wallac) with a 531 nm excitation filter and 595 nm emission filter. Serial dilution data were fit by non-linear regression to provide 50% inhibitory concentrations (IC_{50} values). The effect of test compounds on RNA unwinding catalyzed by human RNA helicase A was measured using the same assay conditions as described above for the NS3 helicase domain.

Discussion on the Protein Used. Ideally the structure-based approach would have targeted the full-length NS3/NS4A protein. This is the form of the protein produced in infected cells, and unwinding by the full-length protein is mechanistically distinct from that by the isolated helicase domain.[20,21] However, practical considerations dictated that this protein could not be obtained in sufficient quantity for the techniques used and number of compounds tested. Based on available crystal structure, however,[22-24] the conserved RNA binding site which was regarded as the primary target in our campaign is not preserved in the isolated helicase domain vs. the full-length protein. To understand any differences in inhibitor activity against these two forms of the proteins, compounds were routinely profiled in biochemical assays using both, with the helicase domain assay being the most relevant comparison with structural and biophysical experiments which used this same protein, and the NS3/NS4A-catalyzed RNA unwinding assay being more physiologically relevant. Further improvements in potency and optimization of the series described herein should apply both assays.

Compound-RNA Interaction. A Sybr Green II – tRNA binding assay was used to evaluate whether compounds interact with RNA. Sybr Green is an RNA-binding dye; it's fluorescence is quenched when bound to RNA, and therefore an increase in fluorescence is observed if test compounds bind to RNA and displace the dye. Assays were performed in 384-well plates in a volume of 10 uL. SybrGreen II (Invitrogen) was used at an 8000-fold dilution of the purchased stock solution and rRNA (Roche) was present at 2 μg/mL. Fluorescence was measured using a VictorII multi-mode plate reader (Wallac) with 340 nm excitation and 405-410 nm emission filters. Either the % of fluorescence increase measured in the absence of tRNA, or for serial dilutions the compound concentration giving 50% of the maximal fluorescence increase was reported.

Determination of Inhibitor Affinity by Isothermal Titration Calorimetry (ITC). The calorimetry experiment was carried out using the VP-ITC microcalorimeter (Microcal Inc.) at a temperature of 22°C. NS3 helicase was exchanged into a buffer consisting of 25 mM Tris, 300 mM NaCl, and 0.5 mM TCEP, 5 mM MgCl2, 3% glycerol, 1 mM EDTA, 0.01% IGEPAL ca-630, plus 5% DMSO final. Inhibitor x was diluted from a DMSO stock solution to give a solution at 300 μM in the same buffer/DMSO mixture. Both solutions were degassed, then the inhibitor solution was spun in a microfuge for 5 min at maximum speed, to remove any particulate matter. The concentration of the protein solution after filtration was determined to be 35 μM by absorbance at 280 nm (based on a predicted absorbance of 0.93 for a 1 mg/mL solution). An initial 2 μl injection was followed by a series of 27 10 μl injections at a spacing of 360 s. Data were fit using Origin (version 5.0, Microcal Inc.), to a one-binding-site model, after correcting the signal for background heat of dilution.

Determination of Inhibitor Affinity by Circular Dichroism (CD) Spectroscopy. CD spectra were acquired on a J-715 spectropolarimeter (Jasco) using a 1 cm pathlength cell without temperature control. NS3 helicase and compound x were prepared in one of two buffers: the pH 7.5 buffer described above for ITC, or a simplified pH 6.5 buffer based on that used for enzymatic assays, but lacking oligonucleotides, ATP, BSA and RNAsin. Titration solutions contained 8.6 μM NS3 helicase and 0-80 μM compound x. CD spectra were acquired over a range from 250-350 nm with a band width of 5 nm, response time of 0.25 sec, and speed of 100 nm/min (10 accumulations averaged per condition). Spectra of 80 μM compound x in the absence of protein were acquired in each buffer, but no significant difference was observed from that for buffer alone. The effects of compound on the NS3 helicase CD spectrum were quantified by plotting the change of the peak signal vs. compound concentration, approximately 264 and

270 nm for the pH 7.5 and pH 6.5 titrations, respectively. The actual values used were the average signals from 2 nm below to 2nm above the peak value to reduce the effect of signal noise. The signal difference vs. compound concentration data were fit by nonlinear regression to a one binding site model using Prism (GraphPad). Fitted parameters K_d and maximum signal change are reported ± the standard error on the fit as determined by the software.

Crystallization, Soaking and Cryofreezing. NS3 Helicase (NS3deltaNM construct) containing uncleaved N-terminal His-tag was used for all crystallization trials. Protein was prepared by exchanging the stock buffer to 10mM Hepes pH 7.5, 1mM TCEP, 1mM EDTA using PD10 column, concentrated to 14.7 mg/mL (A280) and stored in 25ul aliquots at -80C. Freshly thawed protein stock was diluted in the stock buffer to a concentration of ~ 12mg/ml before setting crystallization trials.

Apo HCV Helicase crystals are grown using following protocol. A seed stock was made from crushing from two large crystals (200-250 micron) in 50uL of well solution along with seed bead. This stock was diluted by addition of 400uL of the well buffer and dispensed into aliquots and storing at -80°C for future use. Hanging drop vapor diffusion was used with a well solution of 3.5→4.5% PEG4000, 20mM Sodium Cacodylate pH 5.75 - 6.0, 50 mM Calcium Chloride Dihydrate. The protein drop was added with well solution in 1:1 ratio and incubated at 4°C. Variable volumes of 0.15, 0.2, or 0.3 uL of 5% seed solution were added to the drops. Crystals appears in 2-4 days; matures in 10 days. Optimal number of crystal nucleation can be achieved by serial dilution and optimization of the seed stock.

Harvested apo crystals were crosslinked by equilibrating 4 uL hanging drops over 8 uL of 25% aqueous Glutaraldehyde solution (Sigma, Cat. # G5882) in micro bridges for 90 minutes.

Crosslinked crystals were thoroughly washed iteratively (4x) with 30 uL of cryo-protectant buffer 6% PEG 4000, 25% glycerol, 50mM Na cacodylate pH 6.5, 50 mM CaCl2 before initiating the soaking experiments. Cross linked, washed crystals were transferred to a sitting drop reservoir containing and cryo-protectant buffer containing up to 100 mM fragment of interest. All experiments were performed in 4 °C. On case to case basis, soaking time was reduced to 30-40 minutes or 2 minutes or reduced fragment concentration of 20 mM to 50 mM or apo crystals soaked without crosslinking as may be required to sustain reasonable diffraction quality. Typically soaked crystals were harvested in 2-3 days for data collection by plunge freezing in liquid nitrogen.

Data collection and refinement: Diffraction data were collected at Swiss Light Source synchrotron beamlines PXI or PXIII with marCCD detector under standard cryogenic conditions. For compound **3**, single wavelength anomalous dispersion experiment was conducted at an X-ray wavelength 0.91 Å near the bromine absorption peak. Data were reduced using d*TREK. Structures of ligand co-complexes were determined by using apo HCV helicase as a starting model and calculating difference Fourier synthesis map to determine the electron density for the ligand. Iterative rounds of manual model building using COOT[30] combined with refinement using PHENIX[31] generated final models. All crystal structure figures were generated using PyMOL. The co-complex structure of HCV helicase with compound **2** was determined at a resolution limit of 2.30 Å and refined to Rfree/Rwork statistics of 0.30/0.23. The co-complex structure of HCV helicase with compound **3** was determined at a resolution limit of 2.20 Å and refined to Rfree/Rwork statistics of 0.32/0.26. The co-complex structure of HCV helicase with fragment **1** was determined at a resolution limit of 2.25 Å and refined to Rfree/Rwork statistics of 0.30/0.25. The co-complex structure of HCV helices with compound **7** was determined at a

resolution limit of 2.30 Å and refined to Rfree/Rwork statistics of 0.31/0.25. The co-complex structure of HCV helicase with compound **9** was determined at a resolution limit of 2.15 Å and refined to Rfree/Rwork statistics of 0.30/0.24. The co-complex structure of HCV helicase with compound **13** was determined at a resolution limit of 2.40 Å and refined to Rfree/Rwork statistics of 0.31/0.26. The co-complex structure of HCV helicase with compound **19** was determined at a resolution limit of 2.25 Å and refined to Rfree/Rwork statistics of 0.27/0.22.

NMR Experiments. Samples for STD-NMR experiments consisted of a total volume of 500 μL in deuterated buffer containing 20 mM deuterated Bis-Tris, pH 6.5, 30 mM NaCl, and 1 mM deuterated DTT. The generic fragment library comprised of ~1000 carefully-selected, small fragments (MW < 300) that were highly soluble and tested for self-aggregation properties. The primary screens of the library consisted of the preparation of samples that each comprised a mixture of 3 fragments at 300 μM and HCV helicase at 3.5 μM. NMR experiments were run for each sample where a 1D ^{1}H NMR spectrum was acquired along with a 1D STD-NMR spectrum. The short ^{1}H experiment took less than 2 minutes and provided for a quick *in-situ* quality check and reference phases for the STD-NMR experiment. The STD-NMR experiment used a 2 seconds RF irradiation of Gaussian pulse trains on- (-0.46 ppm) and off-resonance (-20.2 ppm) in interleave scans respectively, with a total experimental time of 55 minutes. The presence of STD signals from the mixture in the sample is indicative of binding of one or more of the fragments to the target protein. A follow-up screen in the simplex format was then performed to deconvolute the potential hits from the mixture. Soaking of the fragment hits in a high-throughput crystallography process was carried out to obtain the binding modes of these fragments, and structure-guided fragment hit optimization would ensure if the binding mode, ligand efficiency and chemistry potential are deemed attractive.

Surface Plasmon Resonance (SPR). Fragment binding to the protein target in the SPR based binding screen was measured in real time as a change in mass in a hydrogel close to the surface of a sensor chip. The signal (expressed in resonance units, RU), which is dependent upon the size and immobilization level of the target, increases with the molecular weight of the fragment and the number of available binding sites. This methodology provides the advantage of consuming low amounts of target protein and fragments. The instrument's automation and throughput also made it well-suited for the mid-scale secondary screening applications of fragment hit confirmation and prioritization for crystallization studies.

SPR experiments were performed on a Biacore® S51 instrument (GE Healthcare) employing a Series S CM5 sensor chip. The N-terminal His-tagged NS3 Helicase (NS3 deltaNM construct) was diluted into the immobilization buffer (10mM sodium acetate pH 6.0) and immobilized to the sensor chip surface via amine coupling chemistry. The carboxylic acid groups on the dextran sensor chip surface were first activated with a mixture of 1-ethyl-3-(dimethylaminopropyl)-carbodiimide hydrochloride and N-hydroxysuccinimide (Amine Coupling Kit, GE Healthcare). The target protein was then injected over the activated surface at a concentration of 30 µg/ml and a flow rate of 5 µl/min to immobilize approximately 13,000 RU of protein. The immobilization running buffer was 10mM HEPES, 150 mM NaCl and 0.005% Surfactant P20. After amine coupling of the protein was complete the remaining active succinimides on the surface were deactivated by injection of 10mM ethanolamine (Amine Coupling Kit, GE Healthcare). The percentage of active protein immobilized was calculated from the saturation response of reference compounds of known affinities. The equilibrium dissociation constants (KD) of these reference compounds were also characterized. The

characterization of these reference compounds validated the binding integrity of the target protein after immobilization.

Fragment samples were obtained in powder form and dissolved in DMSO. The fragment DMSO solutions were dispensed into the running buffer to obtain aqueous fragment solutions containing 20 mM Bis-Tris-HCl pH 6.5, 30 mM NaCl, 0.5 mM TCEP, 0.005% Surfactant P20 and 5% DMSO. Prepared solutions were injected at a flow rate 30 µl/min over the immobilized protein and a control reference unmodified dextran sensor chip surface with a contact/association time of 30 s and a dissociation time of 200 s. This was followed by an extra wash of the flow system with 50% DMSO. The extended dissociation time and 50% DMSO wash were intended to ensure regeneration of the protein surface and minimize cross contamination between samples. Periodically throughout the SPR fragment screen, a well-characterized active site inhibitor and also a sample of only buffer were injected as positive and negative controls to monitor the signal to noise, protein surface stability and binding capacity. Screens were run in a 96-well format and performed at 25 °C. Fragments were evaluated at single concentration of 200µM and then in subsequent dose dependent experiments at concentrations of 200 and 400µM. Report points, taken at the end of the 30 s association phase, were used for the analysis. The brief contact/association period was adequate for this analysis since equilibrium is reached almost instantly with fast on- and off-rate fragment binders and this also reduces the risk of nonspecific binding events during the injection. Data evaluation included reference control dextran surface subtraction, molecular weight adjustment and solvent correction. Our criteria for identifying a protein target binder included the fragment having a binding response level/report point above background (average response of buffer injections + standard deviation) in the single concentration run and then exhibiting reproducible and dose-dependent binding in the dose-

dependent run. Binding sensorgrams were also examined to eliminate fragments demonstrating super-stoichometric binding ($R > R_{max}$) or atypical binding kinetics. Prioritized fragments were further evaluated in a concentration series for affinity-based ranking to triage binders for crystallization trials.

ASSOCIATED CONTENT

Supporting Information

Supporting Information section is available that describes bioinformatics pocket analyses and additional NMR experiments. This material is available free of charge via the Internet at http://pubs.acs.org.

PDB ID CODES

PDB coordinates have been deposited and ID codes are pending.

AUTHOR INFORMATION

Corresponding Information

* Address correspondence to stevenrlaplante@gmail.com and RESGeneral.LAV@boehringer-ingelheim.com. Present address SRL: NMX Research and Solutions Inc., INRS University

(Institut Armand-Frappier), 500 boulevard Cartier Ouest, Suite 6000, Laval, Québec, Canada H7V 5B7.

Notes

The authors declare no competing financial interest.

ACKNOWLEDGEMENTS

We thank the following colleagues for help and discussions: R. Bethell, P. Beaulieu, M. Cordingley, N. Farrow, G. Kukolj, J. Proudfoot and F.S. Farmer. We also acknowledge the valuable teamwork of our colleagues at Boehringer Ingelheim.

ABBREVIATIONS USED

ALI, alternative lead identification; AMU, atomic mass units; CD, circular dichroism; clogP, calculated partition coefficient in octanol:water; DLB, differential line broadening; DMF, dimethylformamide; dsRNA, double-strand RNA; FBDD, fragment-based drug discovery; FBS, fragment based screening; GT, genotype; HBA, hydrogen bond acceptor; HBD, hydrogen bond donor; HCV, hepatitis C virus; HPLC, high performance liquid chromatography; HTS, high throughput screen; IFN, interferon; ITC, isothermal titration calorimetry; LE, ligand efficiency - RTln(IC_{50}) / #heavy atoms; MW, molecular weight; NMR, nuclear magnetic resonance; NS, non-structural protein; POC, percentage of control inhibition; SAR, structure-activity relationship; PASS, Putative Active Site with Spheres; SPR, surface plasma resonance; STD,

saturation transfer difference spectroscopy; TBAF, tetra-n-butylammonium fluoride; THF, tetrahydrofuran; TROSY, transverse relaxation Overhauser spectroscopy.

REFERENCES

(1) (a) Lavanchy, D. The global burden of hepatitis C. *Liver Int.* **2009**, 29**,** 74-81 (b) Ryan, K.J.; Ray, C. G. (eds), An introduction to infectious deseases, *Sherris Medical Microbiology* (4th ed.). 2005, McGraw Hill. 551-552.

(2) Choo, Q. L.; Kuo, G.; Weiner, A. J.; Overby, L. R.; Bradley, D. W.; Houghton, M. Isolation of a cDNA clone derived from a blood-borne non-A, non-B viral hepatitis genome. *Science* **1989**, *244***,** 359-362.

(3) Ghany, M. G.; Strader, D. B.; Thomas, D. L.; Seeff, L. B. American Association for the Study of Liver Diseases. Diagnosis, Management, and Treatment of hepatitis C: An Update. *Hepatology,* **2009**, *49***,** 1335-1374.

(4) (a) Pearlman, B. L. Protease inhibitors for the treatment of chronic hepatitis C genotype-1 infection: the new standard of care. *Lancet Infect. Dis.* **2012**, *12,* 717-728. (b) See for example, LaPlante, S.R.; Nar, H.; Lemke, C.; Jakalian, A.; Aubry, N.; Kawai, S. Ligand Bioactive Conformation Plays a Critical Role in the Design of Drugs That Target the Hepatitis C Virus NS3 Protease, *J. Med. Chem*., **2014**, in press, DOI: 10.1021/jm401338c. Special HCV therapies issue.

(5) Sarrazin, C.; Zeuzem, S. Resistance to direct antiviral agents in patients with hepatitis C virus infection. *Gastroenterology* **2010**, *138***,** 447-462.

(6) Welsch, C.; Zeuzem, S. Will interferon-free regimens prevail? *Gastroenterology* **2012**, *142*, 1351-1355.

(7) Moradpour, D.; Penin, F.; Rice, C. M. Replication of hepatitis C virus. *Nat. Rev. Microbiol.* **2007**, *5*, 453-463.

(8) (a) Sofia, M. J.; Chang, W.; Furman, P. A.; Mosley, R. T.; Ross, B. S. Nucleoside, nucleotide, and non-nucleoside inhibitors of hepatitis C virus NS5B RNA-dependent RNA-polymerase. *J. Med. Chem.* **2012**, *55*, 2481-2531. (b) See for example, LaPlante, S.R.; Bos, M.; Brochu, C.; Chabot, C.; Coulombe, R; Gillard, J.R.; Jakalian, A.; Poirier, M.; Rancourt, J.; Stammers, T.; Thavonekham, B.; Beaulieu, P.L.; Kukolj, G.; Tsantrizos, Y.S. Conformation-Based Restrictions and Scaffold Replacements in the Design of HCV Polymerase Inhibitors: Discovery of Deleobuvir (BI 207127). *J. Med. Chem*., **2014**, in press, DOI: 10.1021/jm4011862. Special HCV therapies issue.

(9) Thibeault, D.; Maurice, R.; Pilote, L.; Lamarre, D.; Pause, A. In vitro characterization of a purified NS2/3 protease variant of hepatitis C virus. *J. Biol. Chem.* **2001**, *276*, 46678-46684.

(10) Pallaoro, M.; Lahm, A.; Biasiol, G.; Brunetti, M.; Nardella, C.; Orsatti, L.; Bonelli, F.; Orru, S.; Narjes, F.; Steinkuhler, C. Characterization of the hepatitis C virus NS2/3 processing reaction by using a purified precursor protein. *J. Virol.* **2001**, *75*, 9939-9946.

(11) Li, K.; Frankowski, K. J.; Belon, C. A.; Neuenswander, B.; Ndjomou, J.; Hanson, A. M.; Shanahan, M. A.; Schoenen, F. J.; Blagg, B. S.; Aube, J.; Frick, D. N. Optimization of potent hepatitis C virus NS3 helicase inhibitors isolated from the yellow dyes thioflavine S and primuline. *J. Med. Chem.* **2012**, *55*, 3319-3330.

(12) Mukherjee, S.; Hanson, A. M.; Shadrick, W. R.; Ndjomou, J.; Sweeney, N. L.; Hernandez, J. J.; Bartczak, D.; Li, K.; Frankowski, K. J.; Heck, J. A.; Arnold, L. A.; Schoenen, F. J.; Frick, D. N. Identification and analysis of hepatitis C virus NS3 helicase inhibitors using nucleic acid binding assays. *Nucleic Acids Res.* **2012**, *40***,** 8607-8621.

(13) a) Pyle, A. M. RNA helicases and remodeling proteins. *Curr. Opin. Chem. Biol.* **2011**, *15***,** 636-642. b) Liu, D.; Wyss, D.F. Backbone 1H, 15N and 13C resonance assignments of the NTPase subdomain of the hepatitis C virus NS3 RNA helicase, *J. Biomolecular NMR* **200**1, *19*, 283-284. c) Gesell, J.J.; McCoy, M.A.; Senoir, M.M.; Wang, Y.S.; Wyss, D.F. NMR-based Screening applied to drug discovery targets, Modern Magnetic Resonance, G.A. Webb, (ed,), Springer, **2006** 1401-1410. d) Boguszewska-Chachulska, A.M.; Krawczyk, M; Najda A; Kopańska K; Stankiewicz-Drogoń A; Zagórski-Ostoja W; Bretner M. Searching for a new anti-HCV therapy: Synthesis and properties of tropolone derivatives, *Biochemical and Biophysical Research Communications,* **2006**, *341*, 641-647. e) Borowski, P; Schalinski, S; Schmitz H. Nucleotide triphosphatase/helicase of hepatitis C virus as a target for antiviral therapy, *Antiviral Res.* **2002**, *55*, 397-412. f) During the course of fragment expansion, a patent application was issued with overlapping chemical matter leading to the deprioritizing of further efforts See: Beigelman, B, Buckman, B. Wang, G, Matulic-Adamic, J., Stoycheva, A. D.; Andrews, S.W., Misialek, S. M.l Rajagopalan, P. T., Fryer, A. M., Gunawardana, I., Haas, J.; Huang, L., Maduru, M. R. Zhang, G., Kossen, K., Serebry, V. Novel Inhibitors of Hepatitis C Virus Replication, *WO 2008/100867*, **2008**.

(14) a) Cheng, W.; Arunajadai, S. G.; Moffitt, J. R.; Tinoco, I., Jr.; Bustamante, C. Single-base pair unwinding and asynchronous RNA release by the hepatitis C virus NS3 helicase. *Science,*

2011, *333***,** 1746-1749. b) See the Supporting Information for views of each pocket along with summaries of residue conservation based on the bioinformatics analyses.

(15) Albert, J. S.; Blomberg, N.; Breeze, A.L.; Brown, A.J.; Burrows, J.N.; Edwards, P.D.; Folmer, R.H.; Geschwindner, S.; Griffen, E.J.; Kenny, P.W.; Nowak, T.; Olsson, L.L.; Sanganee, H.; Shapiro AB. An integrated approach to fragment-based lead generation: philosophy, strategy and case studies from AstraZeneca's drug discovery programmes, *Curr Top Med Chem*., **2007**, *7,* 1600-29.

(16) Zhang, M.Q.; Wilkinson, B. Drug discovery beyond the 'rule-of-five', *Curr Opin Biotechnol*. **2007**, *18,* 478-88.

(17) Freire, E. Do enthalpy and entropy distinguish first in class from best in class? *Drug Disc. Today* **2008**, *13,* 869-74.

(18) Qiang Z.; Muegge, I. PharmShapeCC: 3D pharmacophore searching against ten trillion combinatorially accessible compounds. *9th International Conference on Chemical Structures,* June 5-9, **2011**, Noordwijkerhout, The Netherlands.

(19) Woody, R.W.; Dunker, A.K. Aromatic and Cystine Side-Chain Circular Dichroism in Proteins, *Circular Dichroism and the Conformational Analysis of Biomolecule*s, **1996**, G.D. Fasman, ed. Plenum Press, New York, 109-158.

(20) Beran, R. K.; Lindenbach, B. D.; Pyle, A. M. The NS4A protein of hepatitis C virus promotes RNA-coupled ATP hydrolysis by the NS3 helicase. *J. Virol.* **2009**, *83***,** 3268-3275.

(21) Ding, S. C.; Kohlway, A. S.; Pyle, A. M. Unmasking the active helicase conformation of nonstructural protein 3 from hepatitis C virus, *J. Virol.* **2011**, *85***,** 4343-4353.

(22) Yao, N.; Hesson, T.; Cable, M.; Hong, Z.; Kwong, A. D.; Le, H. V.; Weber, P. C. Structure of the hepatitis C virus RNA helicase domain, *Nat. Struct. Biol.,* **1997***, 4***,** 463-467.

(23) Yao, N.; Reichert, P.; Taremi, S. S.; Prosise, W. W.; Weber, P. C. Molecular views of viral polyprotein processing revealed by the crystal structure of the hepatitis C virus bifunctional protease-helicase. *Structure,* **1999***, 7***,** 1353-1363.

(24) Appleby, T. C.; Anderson, R.; Fedorova, O.; Pyle, A. M.; Wang, R.; Liu, X.; Brendza, K. M.; Somoza, J. R. Visualizing ATP-dependent RNA translocation by the NS3 helicase from HCV, *J. Mol. Biol.,* **2011***, 405***,** 1139-1153.

(25) Thibeault, D.; Bousquet, C.; Gingras, R.; Lagacé, L.; Maurice, R.; White, P. W.; Lamarre, D., Sensitivity of NS3 serine proteases from hepatitis C virus genotypes 2 and 3 to the inhibitor BILN 2061, *J. Virol.,* **2004***, 78***,** 7352-7359.

(26) Thibeault, D.; Massariol, M. J.; Zhao, S.; Welchner, E.; Goudreau, N.; Gingras, R.; Llinàs-Brunet, M.; White, P. W. Use of the fused NS4A peptide-NS3 protease domain to study the importance of the helicase domain for protease inhibitor binding to hepatitis C virus NS3-NS4A, *Biochemistry,* **2009***, 48***,** 744-753.

(27) Zhang, S.; Grosse, F. Molecular characterization of nuclear DNA helicase II (RNA helicase A), *Methods Mol. Biol.,* **2010***, 587***,** 291-302.

(28) Massariol, M. J.; Zhao, S.; Marquis, M.; Thibeault, D.; White, P. W. Protease and helicase activities of hepatitis C virus genotype 4, 5, and 6 NS3-NS4A proteins, *Biochem. Biophys. Res. Commun,* **2010***, 391***,** 692-697.

(29) (a) LaPlante, S. R.; Carson, R.; Gillard, J.; Aubry, N.; Coulombe, R.; Bordeleau, S.; Bonneau, P.; Little, M.; O'Meara, J.; Beaulieu, P.L. Compound Aggregation in Drug Discovery: Implementing a Practical NMR Assay for Medicinal Chemists, *J. Med. Chem*., **2013**, 56, 5142–5150. (b) LaPlante, S. R.; Aubry, N.; Bolger, G.; Bonneau, P.; Carson, R.; Coulombe, R.; Sturino, C.; Beaulieu, P.L. Monitoring Drug Self-Aggregation and Potential for Promiscuity in Off-target In vitro Pharmacology Screens by a Practical NMR Strategy, *J. Med. Chem.*, **2013**, *56*, 7073–7083.

(30) Emsley, P.; Lohkamp, B.; Scott W. G.; Cowtan K. Features and development of *Coot*. *Acta Cryst. D,* **2010**, *66*, 486-501.

(31) Adams, P. D.; Afonine, P. V.; Bunkóczi, G.; Chen, V. B.; Davis, I. W.; Echols, N.; Headd, J. J.; Hung, L.-W.; Kapral, G. J.; Grosse-Kunstleve, R. W.; McCoy, A. J.; Moriarty, N. W.; Oeffner, R.; Read, R. J.; Richardson, D. C.; Richardson, J. S.; Terwilliger T. C.; Zwart, P. H. PHENIX: a comprehensive Python-based system for macromolecular structure solution. *Acta Cryst. D,* **2010**, *66*, 213-221.

(32) Kim, J.L.; Morgenstern, K.A.; Griffith, J.P.; Dwyer, M.D.; Thomson, J.A.; Murcko, M.A.; Lin, C.; Caron, P.R. Hepatitis C virus NS3 RNA helicase domain with a bound oligonucleotide: the crystal structure provides insights into the mode of unwinding, *Structure*, **1998**, 6, 89-100.

(33) Brady, G.P.; Stouten, P.F.W. Fast prediction and visualization of protein binding pockets with PASS, *Journal of Computer-Aided Molecular Design*, **2000**, *14*, 4, 383-401.

(34) LaPlante, S. R.; Aubry, N.; Bonneau, P. R.; Kukolj, G.; Lamarre, D.; Lefebvre, S.; Li, H.; Llinas-Brunet, M.; Plouffe, C.; Cameron, D. R., Line-broadening and Transferred NOESY as a Medicinal Chemistry Tool for Studying Inhibitors of the Hepatitis C Virus NS3 Protease Domain. *Bioorganic & Medicinal Chemistry Letters*, **2000**, *10*, 20, 2271-2274.

Graphics for Table of Contents: